REPORT DOCUMENTATION PAGE

Form Approved
OMB NO. 0704-0188

1. AGENCY USE ONLY *(Leave blank)*	2. REPORT DATE	3. REPORT TYPE AND DATES COVERED
	12/17/96	Final Report - 9/1/92 to 8/31/96

4. TITLE AND SUBTITLE
Low Voltage Electron Beam Lithography

5. FUNDING NUMBERS
N00014-92-J-1966

6. AUTHOR(S)
R. Fabian Pease, Aaron Baum, James Schneider

7. PERFORMING ORGANIZATION NAMES(S) AND ADDRESS(ES)
Leland Stanford Junior University
857 Serra Street, Suite 260
Stanford, CA 94305-4125

8. PERFORMING ORGANIZATION REPORT NUMBER

9. SPONSORING / MONITORING AGENCY NAME(S) AND ADDRESS(ES)
Department of the Navy
Office of Naval Research
Ballston Tower One
800 North Quincy Street
Arlington, Virginia 22217

10. SPONSORING / MONITORING AGENCY REPORT NUMBER

11. SUPPLEMENTARY NOTES
The views, opinions and/or findings contained in this report are those of the author(s) and should not be construed as an official Department of the Army position, policy or decision, unless so designated by other documentation.

12a. DISTRIBUTION / AVAILABILITY STATEMENT
Approved for public release; distribution unlimited.

12 b. DISTRIBUTION CODE

13. ABSTRACT *(Maximum 200 words)*

The properties of negative electron affinity (NEA) photocathodes have been evaluated as sources in electron beam instrumentation. This characterization has been accomplished in two stages. The first stage, carried out in modified night vision tubes, established that these cathodes have brightness of $1x10^8$ A/cm^2-Sr and energy spreads as low as 50meV. The second stage, still in progress, entailed the construction of a demountable UHV electron gun in order to demonstrate cathode lifetime and stability. Thus for, the cathode his routinely been operated at currents as high as 90nA with no significant delay in emission.

14. SUBJECT TERMS	15. NUMBER IF PAGES
electron beam lithography, negative electron affinity photocathode	16. PRICE CODE

17. SECURITY CLASSIFICATION OR REPORT	18. SECURITY CLASSIFICATION OF THIS PAGE	19. SECURITY CLASSIFICATION OF ABSTRACT	20. LIMITATION OF ABSTRACT
UNCLASSIFIED	UNCLASSIFIED	UNCLASSIFIED	UL

LOW VOLTAGE ELECTRON BEAM LITHOGRAPHY

FINAL REPORT

SUBMITTED TO

OFFICE OF NAVAL RESEARCH
800 NORTH QUINCY STREET
ARLINGTON, VA 22217

ATTENTION: DR. ALVIN M. GOODMAN
CHIEF OF NAVAL RESEARCH
CODE: 114SS, ROOM 607

BY

STANFORD ELECTONICS LABORATORIES
STANFORD UNIVERSITY
STANFORD, CA 94305

CONTRACT NUMBER: N00014-92-J-1966

PERIOD OF PERFORMANCE: SEPTMEBER 1, 1992 TO AUGUST 31, 1996

DR. R. FABIAN PEASE, PRINCIPAL INVESTIGATOR

Final Report for DARPA Contract

The work funded on this contract focused on the investigation of a negative electron affinity (NEA) photocathode as an electron beam source for high-performance instrumentation. The first work on this subject consisted of a study of the salient features of negative electron affinity photoemission. Soon thereafter, an industrial partnership was formed between Intevac, Inc. of Santa Clara, CA (formerly of Palo Alto, CA) and Stanford University. Because NEA photocathodes had been established as the basis for production third-generation night vision technology, the first experimental results we obtained were produced in modified night vision tubes. Performing the initial experiments in sealed vacuum tubes had three practical advantages. First, the long lifetime and high stability of cathodes in a sealed tube environment was already well-characterized because of their use in production night vision technology. Second, the sealed tubes were relatively easily modified with the specialized electron optics (electrostatic electrode system) needed to perform brightness and energy spread measurements. Third, the retrofit of the sealed tubes provided a low-cost method of evaluating multiple cathodes and making a preliminary assessment of the technology's feasibility for high performance electron beam applications. A number of measurements of the properties of NEA cathodes in sealed off tubes were made; these results are summarized in the first two papers published under this contract (see attached) that were presented at the 1995 SPIE Conference in San Diego, CA. These papers describe the methods used to characterize the brightness, energy spread, and angular spread from NEA photocathodes in sealed tubes. Unprecedented brightnesses of 1×10^8 A/(cm^2 sr) were

obtained from emission areas 1.7 μm in diameter, along with energy spreads of between 50-250 meV, which were found to depend on the cathode and the illuminating wavelength. In addition, the emitted electrons were found to have very small lateral momenta – a clear electron-optical advantage. This distribution was compared to a theoretical cosine distribution and was found to be slightly superior, thus helping to resolve an old controversy about the angular spread of NEA emission

A number of theoretical studies have been performed on the physical limits of the operation of NEA photocathodes. One such study presented at the 1995 IEDM in Washington, DC showed that in the limit of extremely high emission currents of greater than 20 microamps drawn from a 0.5 micron diameter emission area, trapped charge at the surface of an NEA photocathode will tend to locally decrease the effective NEA at the surface, thus blocking further emission. This phenomenon can lead to a change in emitted distribution of electrons at the surface in the limit of large trapped charge at the surface. These results compared favorably with the results obtained in sealed tubes.
A second study, presented at the 1996 EPIBN Conference in Atlanta, GA examined the use of an NEA photocathode in a parallel electron beam direct write system. Using a Monte Carlo simulation, the effects of beam spacing and current on beam blurring at the wafer were evaluated for a simple electron optical system designed for 0.1 micron minimum feature size with a nominal beam diameter of 30 nm (for linewidth control). The low energy spread of the NEA cathode allows a large fraction of the current generated by the source to reach the wafer (between 33% and 100%, depending on the configuration); thus, high throughputs corresponding to 2.5 microamps delivered at the wafer may be produced with acceptable beam blurring (less than 10 nm). This study has

formed the basis for ongoing work in the area of parallel electron beam emission from an NEA cathode.

Based on the fact that these measurements had established that NEA photocathodes have brightnesses comparable to and energy spreads superior to advanced field emission sources, a decision was made to construct a differentially pumped, demountable UHV electron gun system with the ability to evaluate the sensitivity of NEA cathodes to contamination in a more realistic vacuum environment (i.e., with a sample chamber at 10^{-6} Torr), activate cathodes *in situ*, and replace cathodes with the system still under vacuum. Preliminary design of this system began in July 1995, and construction began in November 1995. To date, NEA photocathodes have successfully been activated to negative electron affinity with high quantum efficiencies of more than 20%. In addition, the electron gun portion of the system has been constructed and is currently being evaluated. In over seven weeks of operation, up to 80 nA of emission have been produced with no discernable decay in cathode emission current over this period. Preliminary stability data shows constant emission (to within an accuracy of 1%) over three days of measurement. Electron-optical imaging of the cathode surface, with the objective of measuring emission area, has been achieved, though further improvements in resolution are planned to ensure the accuracy of brightness measurements. Once this is accomplished, an extensive evaluation of cathode lifetime and stability is planned, as well as measurements of brightness and energy spread on a variety of cathode structures.

After proper focusing of the electron beam is achieved, brightness and energy spread measurements will follow, as well as an extensive evaluation of cathode lifetime and stability.

PROCEEDINGS REPRINT

SPIE—The International Society for Optical Engineering

Reprinted from

Electron-Beam Sources and Charged-Particle Optics

10–14 July 1995
San Diego, California

Volume 2522

Negative electron affinity photocathodes as high-performance electron sources

Part 1: achievement of ultra-high brightness from an NEA photocathode

Aaron W. Baum, William E. Spicer, and R. F. W. Pease
Solid State Electronics Laboratory
Stanford University
Stanford, CA, 94305-4055

Kenneth A. Costello, Verle W. Aebi
Intevac, Inc. Advanced Technologies Division
601 California Avenue
Palo Alto, CA 94305

ABSTRACT

Brightness, energy spread and emission area are key parameters of electron sources for instruments such as electron microscopes and electron beam lithography tools. In developing transmission-mode NEA photocathodes as sources for these applications, these characteristics have been measured in specialized sealed tubes. Average lateral energies were measured at 63 meV for a 1.5 micron thick photocathode, and 83meV for a 0.5 micron thick photocathode, which was known to be emitting "hot" electrons. A current density of 841A/cm^2 was obtained from a 1.7 micron diameter emission area. This high current density can be explained in terms of lateral drift and diffusion of surface trapped electrons. Combined angular and current density data indicate a brightness of ~10^8A/cm^2-sr at 3kV.

Keywords: negative electron affinity, GaAs, Cs, brightness, energy spread, emission area, angular distribution

1. INTRODUCTION

The emission of photostimulated electrons from a negative electron affinity surface was first demonstrated by Scheer and Van Laar 1969.[1] Since then, many applications have developed which take advantage of unique characteristics of negative electron affinity photocathodes — their high quantum efficiency in detectors and night vision,[2] and their ability to produce copious beams of spin-polarized electrons at low energy spreads in high-energy physics[3], and magnetic studies experiments.[4 5] NEAPCs have other advantages as electron sources — picosecond-scale switching time,[6] nearly shot-noise limited emission,[6] and potentially high brightness due to low angular spread of the emitted electrons. [6 7 8]

The basic principle of negative electron affinity electron emission is illustrated in Figure 1. The photocathode consists of a semiconductor, usually a III-V compound such as GaAs, heavily p-doped (1-5x10^{19}) so as to raise the conduction band relative to the Fermi level. The clean semiconductor surface is coated with a layer of Cs and O a few monolayers thick. This activation layer lowers the work function so that the conduction band in the bulk is above the vacuum level — a condition of negative electron affinity. If electrons are excited into the conduction band within a diffusion length (typically a few μm) of the surface, many of them will diffuse to the surface where they will have a high probability of escaping into vacuum.[9 10]

NEAPCs have several characteristics that make them potentially attractive as high-performance electron sources for electron beam microscopy and lithography. They are naturally large-area and planar (cm^2), with uniform emission over their surface.[6] Transmission-mode photocathodes also have the potential for small emission areas (less than 1 micron), determined by diffraction-limited imaging of light onto the photocathode. This is an important property if the cathode is to be used in microscopy or lithography. Coupling these advantages leads to a tantalizing prospect — the emission of multiple, independently-controlled electron beams from a cathode surface. This possibility, coupled with the low energy spread and the high brightness indicated by the results presented in these two papers, motivate the NEXT E project —

0-8194-1881-1/95/$6.00

Negative Electron affinity eXtended area Transmission-mode Emitter — a research and development effort to use NEAPCs for high-performance electron beam lithography and microscopy.

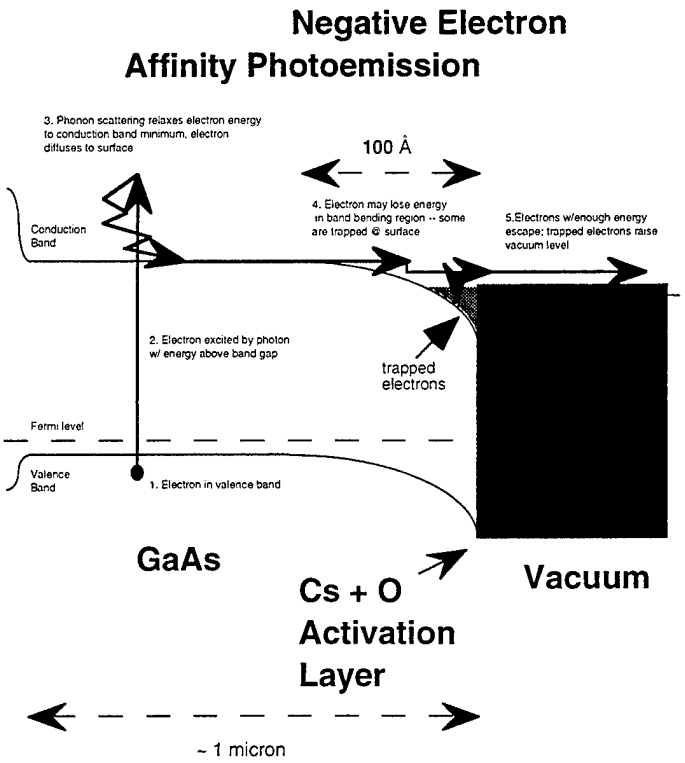

Figure 1. Band diagram of NEA Photocathode, with schematic of escape process

As part of this project, the characteristics of NEAPCs key to electrons source technology — energy spread, brightness, and emission area — have been measured in specialized sealed tubes constructed by Intevac EO Sensors Co. Construction of a prototype demountable NEA electron gun is planned in the near future. The Intevac tubes incorporate long-lifetime negative electron affinity photocathodes with a shelf life of over 10 years and large area (18mm dia.); by incorporating specially-shaped electrodes into the tubes the energy spread, angular spread, maximum current density and area can all be measured on the same photocathode. Results from earlier tubes of simpler designs will also be discussed.

2. TUBE DESCRIPTIONS

2.1. Basic tube + cathode description

All tubes mentioned in this paper were based on night vision tubes developed by Intevac. The photocathode structure is depicted in Fig. 2. The active region is grown with an AlGaAs electron diffusion barrier and then bonded to an anti-reflection coating and the glass that serves as both the input window and as part of the vacuum envelope. All of the photocathodes were MOCVD-grown with a (100) orientation and p-doped with Zn to the specified levels.

To make a tube, the active region's surface is cleaned and etched in a proprietary process, and is then transferred into a UHV system where the cathode is heat cleaned and the active layer surface is exposed to Cs and O to activate it to NEA in another proprietary process. The cathode structure is then indium sealed onto the input end of a tube. The tubes consist of a stack of annular alumina spacers and kovar electrodes brazed into a cylinder that is ended by an output consisting of an aluminized phosphor coated over a fused fiber optic bundle that carries the image on the phosphor out to a surface where it can be imaged easily. The

electrodes used were of two basic types: simple, annular electrodes that did not extend into the interior volume of the tube, meant to exclude external fields and to define uniform fields within the tube; and specialized electrodes that extended across the tube diameter. The latter electrodes included apertures acting as electron optical elements, for spot size and maximum current measurements, and knife edges, for angular spread measurements, as well as open areas of clear line-of-sight between the cathode and phosphor. The specialized electrodes, as well as the cathode and phosphor, were biased directly by DC power supplies. The annular electrodes were biased by resistor chains, with the resistor values proportional to the electrode-electrode distance to establish as close of an approximation to a uniform field as possible. The resistors were typically 5-10MΩ for ceramics 1-2mm wide.

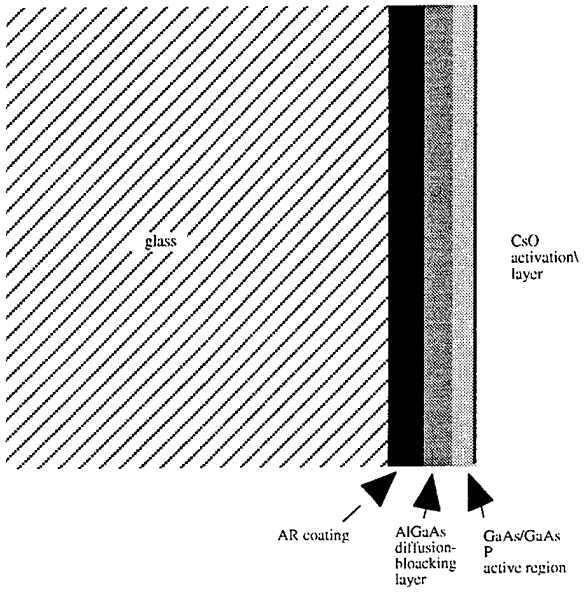

Figure 2. Schematic of transmission photocathode structure.

2.2. Tube Design 1

This tube was intended to measure angular spread, energy spectra, spot size, and maximum current, all on the same cathode. The specialized electrodes are shown in Figure 3. Electrodes 1 and 2 effected a number of two-electrode lenses above the cathode surface, intended to accelerate and either focus or collimate the emitted electrons. The lens used for the emission area and current density measurements is indicated in figure 3; a simulation of this lens in use to focus emitted electrons onto the phosphor is shown in figure 5. A third specialized electrode incorporated a knife edge 8.4 mm from an exposed part of the cathode surface; this edge was used for the angular analysis measurements presented below. Figure 4 illustrates the use of this edge in an angular spread measurement. The phosphor was placed 14mm from the cathode surface. Several of the holes in the electrodes were not used in the experiments described. The specialized electrodes were all made from 5-mil thick kovar stock. The front of the first electrode (the closest to the cathode) was coated with C before the cathode was sealed onto the tube to ensure a uniform work function and prevent charging; this coating was critical for the energy spectrum measurements. The ceramics and annular electrodes were shielded during this evaporation.

2.3. Tube Design 2

Tube design 2 was intended to achieve high magnification imaging of the emitted electrons onto the phosphor. To accomplish this it uses two cascaded lenses, one near the cathode (similar to design 1), and an einzel lens approximately halfway between the cathode and the phosphor. The electrodes leave an area of the cathode with direct line of sight to the phosphor, and angular spread data was derived from the pattern of

electrons striking the phosphor as described below. The distance from cathode to phosphor is somewhat longer, 24.4 mm, than in design 1, facilitating these measurements. The electrode drawings are not shown because the angular data presented here should not depend on the details of the electrode shape.

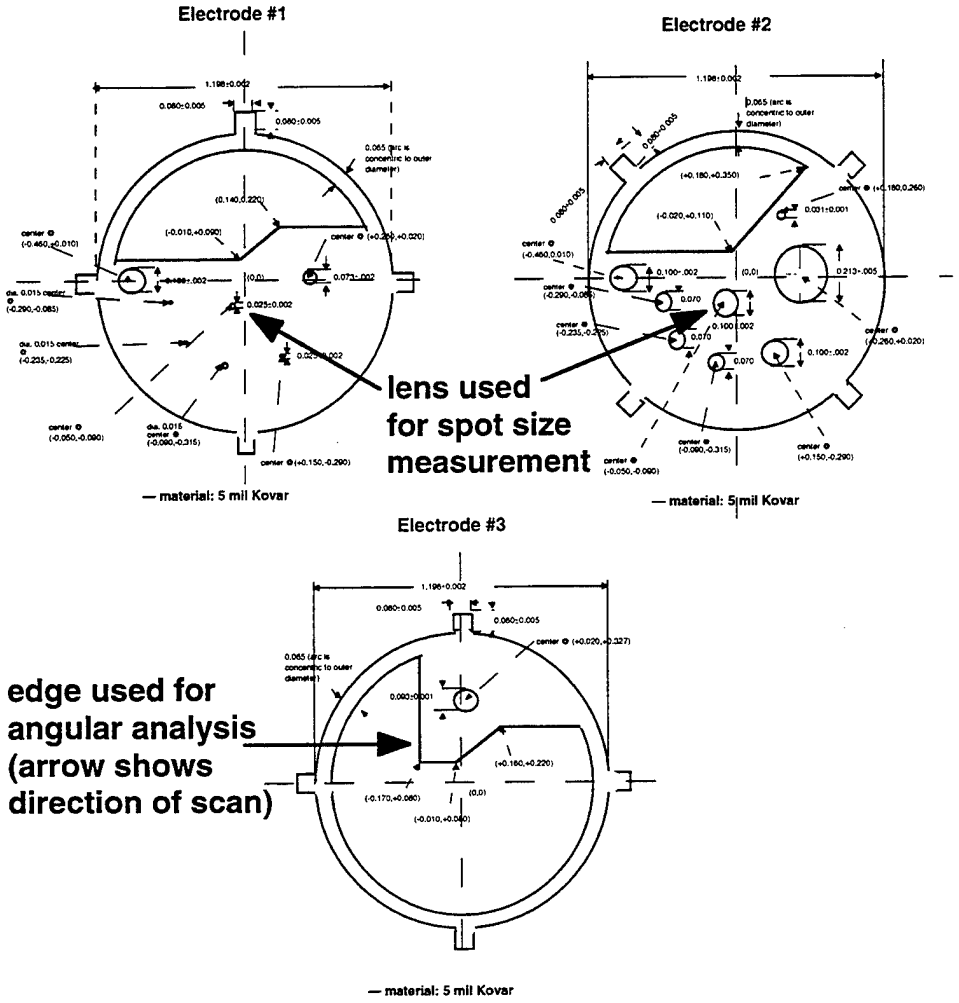

Figure 3. Drawings of Tube Design 1 electrodes. Height in mm of front surface above cathode: Electrode #1: 0.33 ; Electrode #2: 1.40; Electrode #3: 8.36; Phosphor: 14.8.

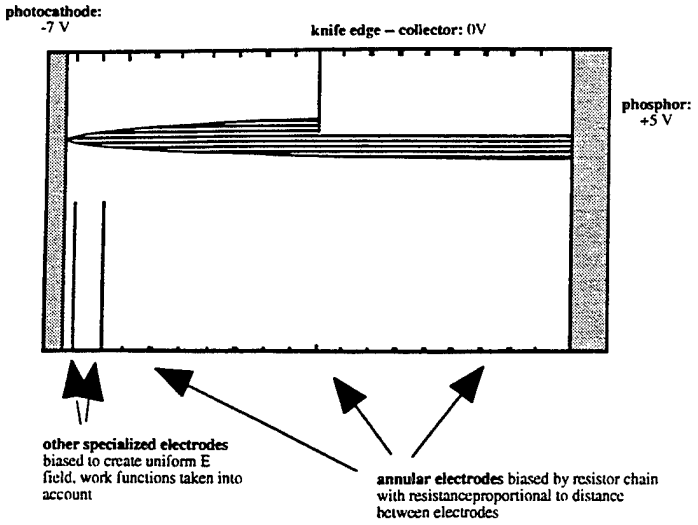

Figure 4. Schematic Depiction of knife-edge angular analysis mode (not to scale).

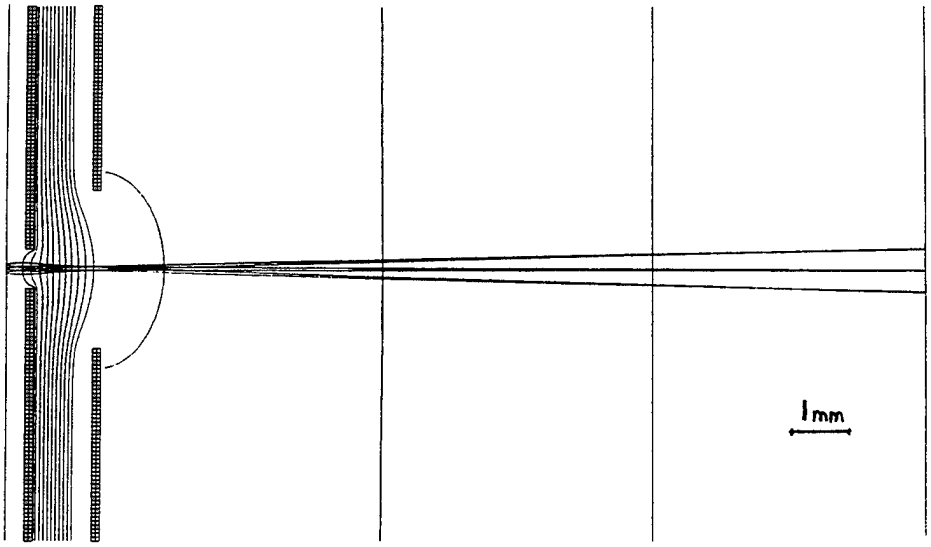

Figure 5. SIMION simulation of center lens in Tube Design #1 imaging cathode surface onto phosphor with 5.4x magnification. 1: photocathode, 0 V. 2: first electrode, ~20 V, adjusted for focus. 3: second electrode, 1500 V. 4: phosphor, 3000 V.

3. EXPERIMENTAL ARRANGEMENT

The experimental setups is illustrated in figure 6. Light from a 5mW HeNe laser or a filtered 100W Hg arc lamp was focused into a microscope objective that then focused the light through a pinhole. A 3 micron diameter pinhole was used for the spot size and angular spread measurements, and pinholes up 100 microns in diameter were used for energy spread measurements, for which the spot size was not as critical. (See figures 4 and 5.) A microscope objective was then used to collect the light from the pinhole and focus it to an intermediate image. This image was then focused onto the photocathode active region by a special two-lens system, designed on SuperOSLO to compensate for the spherical aberration of the 5 mm thick glass substrate of the cathode, which forms part of the tube's vacuum wall. With a 6.3x objective collecting the

light from the pinhole, the final image was nominally demagnified from the pinhole by 3x. The numerical aperture of the system was approximately 0.5. The final lens system could be finely translated in all three axes parallel and perpendicular to the optical axis to achieve the best imaging on the photocathode surface. The tube assembly could also be finely translated in both directions perpendicular to the optical axis.

To shield the tube from magnetic fields, the tube was initially placed in a cylinder made from 100 mil Carpenter high permeability "49" alloy, annealed at 2100°F for 4.5 hours. The final lens was mounted on a snout that screwed into a cap that covered one end of the tube. Both the snout and the cap were made from the Carpenter alloy as well with the same annealing process. The snout held the final lens close to the photocathode, as well as preventing the penetration of magnetic fields through the lens opening. The axial magnetic field near the center of the shielding tube was measured to be less than 10 milligauss regardless of orientation; the construction of the magnetometer prevented measurement of any other components, but they are expected to be equally low. The tubes were also degaussed to eliminate any residual magnetization of the electrodes.

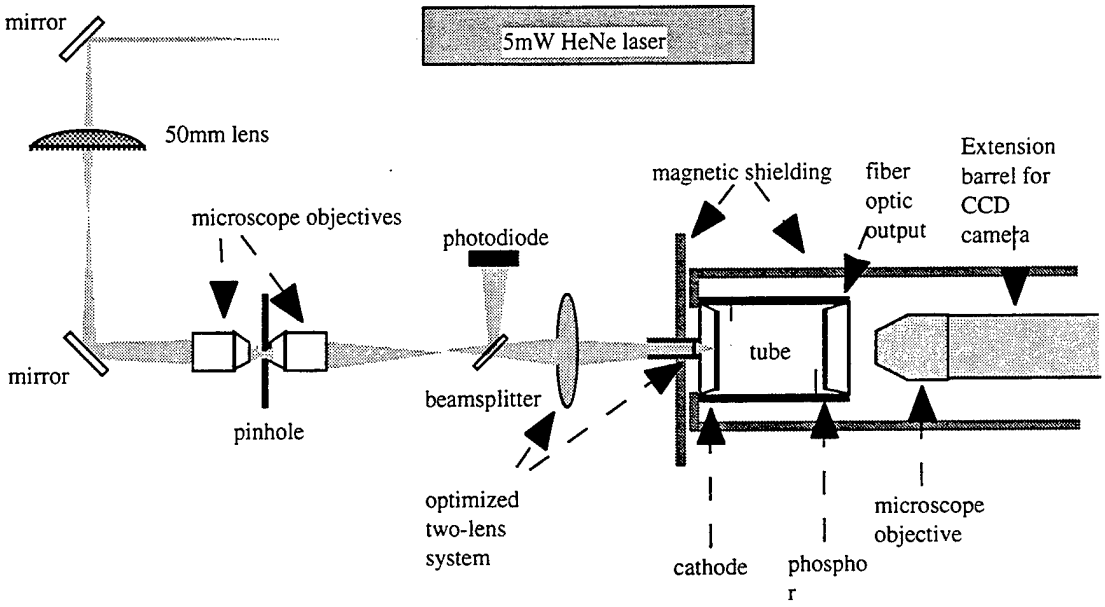

Figure 6. Experimental setup for Mark III tube w/ laser

All experiments were performed in a blacked-out room, with the cathode shielded against any stray light.

When current striking a given electrode was monitored, the illumination was modulated by an optical chopper at 140Hz. The shielded electrode lead was connected to ground through a Keithley preamplifier with a gain of 10^9. After bandpass filtering the signal was measured by a lock-in amplifier. This arrangement minimized noise and drift.

4. BRIGHTNESS

Paraxial brightness, defined as the current density per steradian (A/cm^2-sr) close to the optical axis at a given voltage, is a crucial parameter of any electron source, and for high-performance electron beam systems it must be as high as possible. Thermal field emission electron sources now used in such systems can attain brightnesses of approximately 10^7-10^8A/cm^2-sr at 3kV accelerating voltage. The best available brightness data from NEA photocathodes previous to this work is that of Sanford, who measured a DC. brightness of roughly $5x10^5$ A/cm^2-sr at 3kV from an emission area of approximately 15 microns diameter.[6] This source size and brightness are inadequate for the most demanding applications, such as metrology and lithography in the semiconductor industry.

The brightness of an electron source depends on two key factors: the current density at the cathode surface and the angular distribution of the emitted electrons. Separate techniques were used to measure these two factors, and then the data were combined to determine the brightness.

4.1. Angular Distribution

When the electrons enter into the surface depletion region, they have thermal energies (i.e. on the order of kT). In the depletion region, the electrons are accelerated only in the direction normal to the surface — i.e., their lateral energy is not affected by the built-in field. Thus it might be expected that the electrons would be emitted with lateral energies on the order of kT. Several mechanisms intervene, however, to change this picture. Scattering from phonons in this region can randomize the momentum gained from the built-in fields, increasing the lateral energy spread. At the surface the electrons' lateral energy may be reduced by quantum refraction; if the interface is sufficiently smooth, the sudden change in quantum-mechanical wavelength should deflect the electron's momentum toward the surface normal.[7] According to the idealized theory, the energy of the electron's lateral motion should be reduced by the ratio of the electron's effective mass to its vacuum mass. An uneven activating layer or semiconductor-activator interface could lessen or eliminate this effect. Finally, the electrons may suffer scattering within the activation layer, which is widely believed to be amorphous. [11]

To measure the angular distribution of the emitted electrons, two different techniques were used. In both cases a small spot (~several microns) on the cathode surface is illuminated in an area which is in direct line-of-sight to the phosphor. A uniform electric field is created within the tube by appropriate biasing of the electrodes (specialized and annular), cathode, and phosphor so that the electrons follow parabolic trajectories.

In the first technique, carried out in tube design 1, the tube is translated across the light beam so that an edge of the third electrode (8.36 mm above the cathode) cuts across the beam. The current absorbed by the knife edge is measured vs. position, then differentiated and both axes were scaled to obtain the presented data (figure 7). 10-50pA of current were used for the measurements. The photoemission efficiency of the photocathode was measured to be constant within ±5% in this region. The voltage from the cathode to the knife edge varied from 6 to 12 V. In this case the active region of the cathode was GaAs, 1.5 microns thick, doped $10^{19}cm^{-3}$, activated to approximately 100meV NEA.

In the second, improved technique, performed in tube design 2, the electrons strike the phosphor with energies ranging from 3500-5000eV. The distribution of the light emitted by the phosphor is transmitted by the fiber optic bundle to its back surface, where the pattern is imaged into a CCD camera by a microscope objective attached to a barrel extending from the camera. The video signal is digitized and stored in a computer by means of a frame grabber board; it was then analyzed to obtain the radial distributions presented. The phosphor showed no signs of nonlinearity at the intensities used. From 0.1 to 5 nA of current were drawn to make the measurement; less was drawn for the higher voltages, as the phosphor was more sensitive to higher-energy electrons in this energy range. A typical video image is shown in figure 8. A distribution of current density vs. angle, derived from the video data, for a theoretical acceleration voltage of 3000V is shown in figure 7. In this case the active region of the cathode was GaAs, 0.5 microns thick, doped $8x10^{18}cm^{-3}$, activated to approximately 120meV NEA. The energy spectrum of the cathode was very similar to those of a cathode discussed in Part 2, also 0.5 micron thick with a similar (5%) quantum efficiency at 633 nm. Hot electrons make up a significant portion of both spectra, and may well influence the angular distribution as well, as the hot electrons can enter the band-bending region with lateral energies far higher than those of the thermalized electrons.

The raw data for the knife edge technique suffered from significant asymmetry, especially for the lower accelerating voltages; this effect was likely due to scattered primary and secondary electrons. The light distributions on the phosphor were consistently radially symmetric, and the derived angular distribution showed no variation with voltage in the range used. The former data show an average lateral energy (taking the whole radial distribution into account) of 63meV; the latter show an average of 83meV. This difference is probably due to the presence of hot electrons in the latter's emission; in both cases 633 nm radiation was used, but the thinner cathode's energy spectrum showed a significant amount of hot electrons (c.f. Part 2). Previously other researchers have reported average lateral energies of over 100meV for fully activated GaAs NEA photocathodes[12 13]. Sanford reported an average lateral energy of 31meV. These differences may be

due to differences in measurement technique, experimental error, or to differences in the heat cleaning and activation; a larger NEA may well lead to larger lateral energies, as more highly scattered electrons can escape the cathode.[8] Other causes could include micropitting [15], or changes in the level of scattering in the activation region.[14]

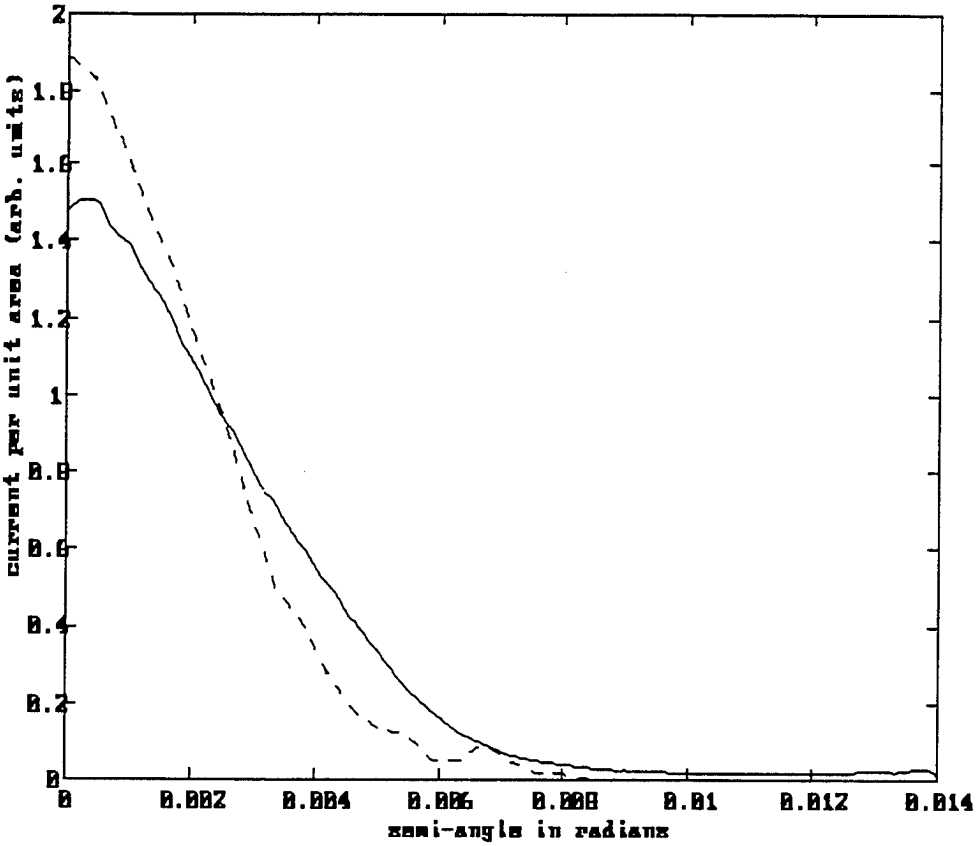

Figure 7. Current density vs. angle, for the knife edge technique in tube design 1 (dashed line), and from the CCD technique using tube design 2 (solid line). Semi angle based on a 3000V accelerating potential and unity magnification.

Figure 8. Typical video image of phosphor in angular analysis mode. 4000V cathode to phosphor. Field of view on phosphor: 952 x 714 microns.

4.2. Spot Size & Current Density

Work by Herrera-Gomez and Spicer into the limitations of current density in nanosecond-pulsed, large area (cm^2), high current (~10A) NEA electron sources found that the key limiting factor was the dipole formed by electrons that are trapped at the surface after losing too much energy to escape from the photocathode.[14] [15] The field caused by this build-up of charge at the surface raises the vacuum level relative to the bulk, lowering the NEA and cutting off the emission of electrons. A simple model of thermionic emission over the band-bending region barrier was found adequate to fit the pulse power vs. current emitted for a GaAs photocathode doped to $2x10^{19}$ cm^{-3} at several different stages of activation.[15] Tunneling of holes through the barrier may also become important in cathodes even more heavily doped.

In our work we concentrate on a different regime: DC emission from a micron- or submicron-sized spot. In this case, the lateral diffusion and drift of the trapped electrons has a far greater role in determining the dipole that cuts off electron emission.

To obtain an order-of-magnitude calculation of the importance of lateral diffusion and drift of the trapped electrons, it is useful to employ a simple one-dimensional model of the trapped electrons. Since the light spot is radially symmetrical, it is natural to use radial coordinates centered on the light spot. Considering an area on the cathode surface of radius r in the steady state, the current flow in and out must be equal, i.e.

$$I_{trap} = q\,R + 2\pi\, r\, q\,(D_{ns}\frac{\partial\sigma(r)}{\partial r} + \mu_{ns}\,\sigma(r)\frac{\partial V_s}{\partial r}), \qquad (1)$$

where I_{trap} is the rate at which electrons are trapped within the radius r, R is the rate of recombination of electrons within the radius r, $\sigma(r)$ is the sheet density of electrons at the radius r, V_s is the voltage on the surface, and D_{ns} and μ_{ns} are the lateral diffusion constant and lateral mobility of the trapped electrons respectively. Let N(r) be the total number of electrons within the radius r. Let V_0 be the voltage at the center of the spot relative to the surface far from the center. Now assume that r is roughly the $1/e^2$ radius of the emission spot. For the purposes of order-of magnitude calculations,

$$\sigma(r) \approx \frac{N(r)}{r^2}, \quad \frac{\partial \sigma(r)}{\partial r} \approx \frac{N(r)}{r^3}, \text{ and } \frac{\partial V_s}{\partial r} \approx \frac{V_0}{r}. \tag{2}$$

Using also the fact that $D_{ns} = \frac{kT}{q} \mu_{ns}$, the drift and diffusion part of equation 1 becomes:

$$2\pi q \left(\frac{kT}{q} + V_0\right) \mu_{ns} \frac{N(r)}{r^2}. \tag{3}$$

Assuming μ_{ns} is 10^{-2} smaller than the bulk mobility, 8800V-cm/s^2, and that $V_0 = 0.2V$ (a typical value for the negative electron affinity), this gives a fractional change of N(r) per second of

$$\frac{57}{r^2}, \tag{4}$$

where r is in cm. This means that for a spot radius of 1μm *all* of the trapped electrons will drift or diffuse out within 0.2 nanoseconds!

The charge density necessary to raise the surface voltage by V is $\sigma = \frac{\varepsilon_s V}{l}$, where l is the width of the band bending region. This equation assumes that all of the trapped charge is concentrated at the surface. For typical doping levels, l = 100 Å, so if V = 0.2V, $\sigma = 2.3 \times 10^{-7}$ C/cm^2. From the above calculations, a 1 micron diameter spot with this electron density would have an outward current flow of 21μA, which translates to a current density of 2622 A/cm^2. In comparison, thermionic emission of holes to the surface can be estimated, in the manner of Herrera-Gomez, by the standard model of a biased semiconductor-metal contact, with zero-current band bending of 0.5 V and a forward bias of 0.2 V; this gives a hole current density two orders of magnitude lower than the lateral current of trapped electrons calculated above. Thus the lateral movement of electrons should be the dominant effect determining the density of the trapped electrons and thus the maximum current density.

Monte Carlo modeling of electron dynamics the band-bending region[16] suggests that the rate of escape into vacuum for electrons in the band-bending region should be comparable to, if not greater than, the trapping rate. Thus current densities of 1000's of A/cm^2 or greater are expected for spot sizes in the micron and submicron range. This should be compared to current densities of ~100 A/cm^2 for the best LaB_6 sources.

A two-dimensional computer model is currently being developed which takes into account the diffusion of electrons in the bulk, the drift and diffusion of the surface-trapped electrons, and the interaction between these two distributions. Initial results are supportive of the results presented here.

The special lens configuration described in the experimental description section above was used to focus light from a 5mW HeNe laser to a small spot on the photocathode centered beneath the electron lens indicated in figure 3. (Tube design 1, with the 1.5 micron thick GaAs photocathode described in the angular analysis section, was used for these measurements.) The emitted electrons were accelerated and focused onto the phosphor, 14.8 mm away. Simulations of the electron optics using SIMION showed a 5.4x magnification of the cathode surface onto the phosphor. (Fig. 5) The voltages used in the simulation agreed well with those used in practice; differences were small enough to be attributable to work function variation, machining errors, and computational errors.

A 16x microscope objective focused the light from the fiber optic output into a CCD camera. This image was sent to a television screen where it was measured. In this way, the smallest spot on the phosphor was estimated to have a $1/e^2$ diameter of 9.4±2 microns. This translates to a 1.7±0.4 micron emission area. The main obstacle to determining the minimum spot size turned out to be the size of the fibers in the bundle; since they are spaced 6 microns center-to-center, estimating the spot diameter was quite risky. The best estimate was obtained by moving the spot around over several fibers and guessing at an average diameter. The fact that the phosphor particles are ~2 microns in diameter should also be noted. Even with all of these uncertainties, it is still clear that the emission area is less than a few microns, a regime of operation that has never before been reported.

The current density achievable in this configuration was then investigated. Keeping the light optics fixed, the electron optics were changed to provide a high (3000V/mm) field at the cathode surface; the cathode was at -20V, the first electrode at 1000V, the second electrode was placed at -10V, and the collector was set to +0V to collect the emitted electrons. In this way it was hoped to minimize electron-stimulated desorption while maintaining a high field on the photocathode. By removing OD filters from the beam, the light level was increased, and the emitted current was measured. The results are shown in Fig. 9. If the diameter of the emission spot is assumed to stay the same as the current is increased, the current density can be approximated by assuming uniform emission over the diameter of the spot (1.7 microns). This technique yields 841A/cm^2 for the highest current level attained. It should be noted that the uncertainty in the spot size translates to an uncertainty of approximately ±50% in the current density; in spite of this, the current densities demonstrated by this measurement are vastly higher than have ever been reported from an NEAPC before. Furthermore, the continuing upward slope of the current vs. light curve indicates that the maximum current density may be much higher than what was measured; the optical setup could not deliver any more optical power to the spot.

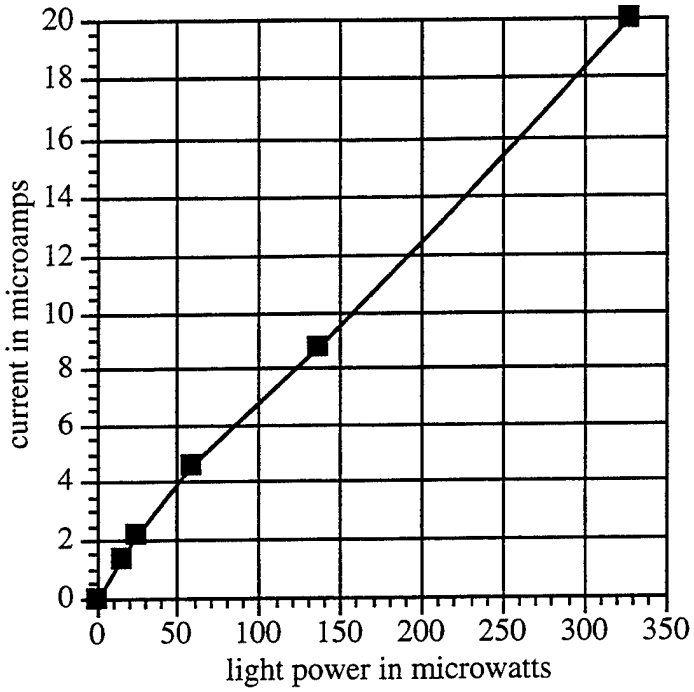

Figure 9. Current vs. 633nm light power for 1.7μm diameter spot

An attempt to measure the spot size and shape vs. current density was made. To do so, the sensitivity of the phosphor-CCD system had to be reduced. This was achieved by reducing the landing energy of the electrons to 3000V, and by employing the electric iris of the CCD camera. The spot size was found to stay constant (~1.7 micron diameter) to within the precision of the technique (~±0.3 microns) from a current of 50 pA up to a current of almost 0.1mA; at around that current level the spot size seemed to increase several times (3-8x) and became asymmetrical. It seems unlikely that this could be an actual increase in emission area size, as the effect of current is expected to rise gradually. The possibility of space-charge interaction outside the cathode is important, as the lens arrangement has only a low field, 165V/mm, above the cathode, where the electrons are tightly-packed and slow-moving; at 0.1mA, for this field, there are an average of 20 electrons in the first 15mm of space above the cathode. For the total current measurements, the field was much higher, over 3000 V/mm.

Tube design 2 incorporates two cascaded lenses to achieve high magnification imaging of the emission spot onto the cathode — up to 96x in simulation. The first lens is similar to that of design 1, but it is designed for operation with a high field (~4000V/mm) on the cathode; it focuses the beam to a magnified real image that is then focused by the second lens, an einzel lens, onto the phosphor. This measurement technique, which should be more accurate and allow measurement at much higher current without the problems of

space charge and nonlinearity of phosphor response encountered using tube design 2. The thinner photocathode (0.5 microns) in this tube should also provide a smaller emission area. Results from this tube are forthcoming.

4.3. Derived Brightness

The results of the knife edge angular analysis and the current density data for the 1.7 micron diameter emission area from the same 1.5micron thick photocathode in tube design 1 were combined to estimate the brightness of such a cathode operating under the condition of an ultrasmall spot size. The data indicate a brightness of at least 10^8 A/cm^2-sr at 3kV, for semi-angles of less than 0.5 milliradians at unity magnification. This angle is specified because typical electron beam systems require probe sizes much smaller than a micron, which will require demagnification that will limit the angular range of the electrons used to a value in this range (<1 milliradian).

5. SUMMARY OF RESULTS

The angular distribution of NEA GaAs photocathodes have been measured in specialized sealed tubes. The results indicate an average lateral energy of 63 meV for a 1.5 micron thick photocathode, and 83meV for a 0.5 micron thick photocathode, which was known to be emitting some "hot" electrons. These average lateral energies are somewhat less than those that have been reported elsewhere.[14 15]

Emission areas of 1.7microns in diameter have been produced and measured on NEA photocathodes. Consistent with a new theory of the lateral movement of trapped electrons, the micron-scale spots show DC current densities far higher than has reported previously -- approximately 841 A/cm^2 at the maximum light power in the experimental arrangement. Significantly higher current densities may be achievable with greater light intensity and/or smaller emission areas. This result, combined with the measured narrow angular spread, indicate a brightness of approximately 10^8A/cm^2-sr, a brightness comparable to that of field emission sources.

This work was supported by the ARPA Advanced Lithography Program under ONR Grant No. N0001492J1996 .

Aaron Baum was supported by an NSF Graduate Fellowship during the period of this work.

---

[1] J.J. Scheer and J. Van Laar, Solid State Comm. **3**(1965) 189-193.
[2] I.P. Csorba, *Image Tubes,* Howard W. Sans& Co, Indianapolis, Ind., 1985.
[3] R. Calabrese, J.M. Gong, V. Guidi, F. Masoli, and L. Tecchio, Nuclear Instruments and Methods In Physics Research **A309**(1991) 21-24.
[4] U. Kolac, M. Donath, K. Ertl, H. Liebl, and V. Dose, Rev. Sci. Instrum. **59**, 1933 (1988).
[5] C.S. Feigerle, D.T. Pierce, A Seiler, and R.J. Celotta, Appl. Phys. Lett. **44**, 866 (1984).
[6] C. A. Sanford, Doctoral Thesis, Cornell University Department of Electrical Engineering, Ithaca NY, (1990).
[7] R.L. Bell, *Negative Electron Affinity Devices*, Clarendon Press, New York, 1973.
[8] Private Communications with Verle Aebi, Intevac, Inc. Advanced Technologies Division.
[9] W.E. Spicer, Phys. Rev **112**(1958), 114.
[10] C.N. Berglund and W.E. Spicer, Phys. Rev. **136**(1964) A1030-A1044; A1044.
[11] B Goldstein, Surf Sci. **47** (1975), 143..
[12] D.C. Rodway and M B Allenson, J. Phys. D: Appl. Phys. **19**(1986) 1353-1371.
[13] D J Bradley, M B Allenson, and B R Holeman, J Phys D:Appl. Phys. **10**(1977), 111-125.
[14] A. Herrera-Gomev and W. Spicer, SPIE Interantional Syposium on Optics, Imaging, and Instrumentation, San Diego, CA, July 1993.
[15] A. Herrera-Gomez, W.E. Spicer, SPIE Vol. 2022, Photodetectors and Power Meters (1993) 51.
[16] Private communications with W.E. Spicer, G. Vergara, and A. Herrera-Gomez.

PROCEEDINGS REPRINT

SPIE—The International Society for Optical Engineering

Reprinted from

Photodetectors and Power Meters II

11–12 July 1995
San Diego, California

Volume 2550

Negative electron affinity photocathodes as high-performance electron sources

Part 2: Energy spectrum measurements

Aaron W. Baum, William E. Spicer, and R. F. W. Pease
Solid State Electronics Laboratory
Stanford University
Stanford, CA, 94305-4055

Kenneth A. Costello, Verle W. Aebi
Intevac, Inc. Advanced Technologies Division,
601 California Avenue
Palo Alto, CA 94305

ABSTRACT

The energy spectra of electrons emitted from transmission-mode negative electron affinity photocathodes have been measured at high resolution using a parallel-plate retarding technique . The spectra from GaAs photocathodes have a basic structure that varies with temperature, activation layer qualities, cathode thickness, and illuminating wavelength. A FWHM energy spread of approximately 50meV at room temperature has been achieved. Spectra from a GaAsP cathode show a markedly different structure and a much wider energy spread.

Keywords: negative electron affinity, GaAs, GaAsP, Cs, energy spectrum, energy spread, electron scattering, angular distribution

1. INTRODUCTION

Negative electron affinity (NEA) photocathodes are being researched as possible high-performance photocathodes for electron beam applications such as microscopy and lithography. For many of these applications, especially microscopy employing low landing voltage (<1kV), the energy spread of the electrons is a key factor affecting resolution. The potentially low energy spread of electrons emitted from NEA photocathodes is thus very attractive, and the need to quantify the factors affecting energy spread is also clear. Another motivation for the measurement of the energy spectra of electrons emitted from these cathodes is that, if sufficient resolution is achieved, much information can be gleaned from the spectra about electron dynamics within the cathode, and the condition of the activating surface.

2. EXPERIMENTAL ARRANGEMENT

The specialized sealed tubes used in these experiments are described in Part 1. The experimental setup shown in Part 1 was used for the presented room temperature data. For the low temperature data, the tube was placed in a PMT cooler, which could lower the temperature of the tube as low as 170K. Because of the thickness of the double-walled window into the cooler, the special lens system described in Part 1 could not be used, and a 50 mm focal length lens was used instead. The arrangement is shown in figure 1. The temperature of the tube was measured with a thermocouple in contact with the tube body. The energy spectra indicated temperature variations if the tube were not given enough time to equalize with the cooler's walls; generally 1 hour of equilibration time was allowed between spectra taken at different temperatures. In all cases the illuminated area on the photocathode was less than 100 microns in diameter

.3. NEA ELECTRON ENERGY SPREAD — DISCUSSION

In a typical NEAPC, electrons are excited by above-bandgap light into the conduction band, where they rapidly relax to a thermalized distribution (after traveling typical distances of ~300A) through interactions with optical phonons.[1] In a transmission-mode photocathode, the absorption length of the light and the cathode thickness (typically ~1 micron) determine the number of electrons that are excited close to the cathode surface; if the active region thickness (henceforth referred to as the cathode thickness) is at least a

few times the absorption length, almost all the electrons reaching the surface will be thermalized into a Maxwell-Boltzmann distribution. If the cathode is not so thick, hot electrons may be observed in the emitted spectrum.

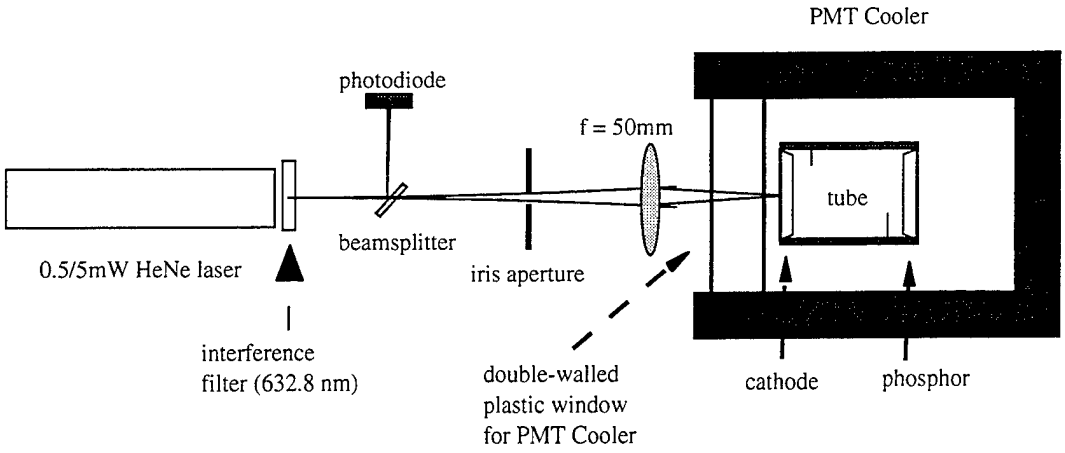

Figure 1. Experimental arrangement with PMT Cooler.

Some of the thermalized electrons may escape without losing energy; these form the higher-energy part of the energy spectrum along with any hot electrons. Many electrons, however, lose energy to phonons in the band-banding region and possibly the activation layer. These form the lower-energy part of the spectrum. The vacuum level, the minimum energy of an electron immediately above the cathode surface, forms a low-energy cutoff for the spectrum; electrons whose energies fall below this level cannot escape.

4. MEASUREMENT TECHNIQUE

All of the energy spectra presented here were obtained using a parallel-plate geometry. High resolution energy spectra have been reported using this technique.[2] The current arriving on the front surface of the first electrode (325 and 570 microns from the cathode for tube designs 1 and 2 respectively) was measured as the voltage between them was varied slowly, obtaining an I vs. V curve. Differentiating this curve, after normalizing for the light level (measured by the beamsplitter and photodiode), obtains the presented energy spectra. To stay as close as possible to a parallel-plate geometry, the beam spot was kept at least a few mm from any holes or edges in the collecting surface, or the edge of the cathode. Work-function variation over the surface of the collector also had to be minimized. This was accomplished in tube designs 1 and 2 with a carbon coating approximately 50nm thick applied to the collector surface before sealing the tube using vacuum evaporation. When either or both of these rules were violated, a low-energy tail sometimes emerged in the energy spectrum.

When the photocathodes were fully activated, very little variation of the energy spectra were seen over the period of measurement for each tube (several days). For the overcesiated cathode presented below, significant movement of the vacuum level, up to 20meV/day, was observed, as the cesium balance on the cathode surface improved.

It should be noted that the parallel-plate geometry only measures the energy of the electrons' motion normal to the cathode surface. Thus, the energy spectra presented are actually the "normal energy" spectra. However, as shown in the angular spread section of Part 1, the electrons emitted from the cathode are at least somewhat "forward-focused"; i.e. many electrons are emitted at angles close to the surface normal. This property of emission would tend to make energy spread measured more similar to the true total energy spread. This idea is supported by the seemingly high resolution of features in the energy spectra. It should

also be noted that energy spectra obtained this way will always give a "pessimistic" — i.e. larger — measure of the emitted electrons' energy spread for electron optics purposes.

5. MEASUREMENTS

5.1. 0.8 micron thick GaAs photocathode — Spectra vs. temperature

The energy spectra of electrons emitted from a GaAs photocathode Zn-doped to ~$10^{19}cm^{-3}$, approximately 0.8 microns thick, were measured at several different temperatures and conditions of the CsO activating layer. Figure 2 shows energy spectra for 215 K and 300 K. The quantum efficiency of the cathode for the 633nm illumination used was 15.7% and 10.6% for 215 K and 300 K respectively. The higher quantum efficiency may be due to a longer diffusion length in the bulk at low temperatures. The electron energy for all the presented spectra is inferred from the low-energy cutoff of the dI/dV curve, which corresponds to the vacuum level. This cutoff is usually fairly sharp (falling to almost zero in less than 30meV). The electron energy for the dI/dV curve is then defined as the difference between the applied voltage and the voltage at which the cutoff takes place. In figure 2, the cathode was assumed to have the same vacuum level at both temperatures, so that the two curves could be compared. This assumption gave the correct value for the movement of the conduction band minimum (CBM) with temperature, to within 5meV.

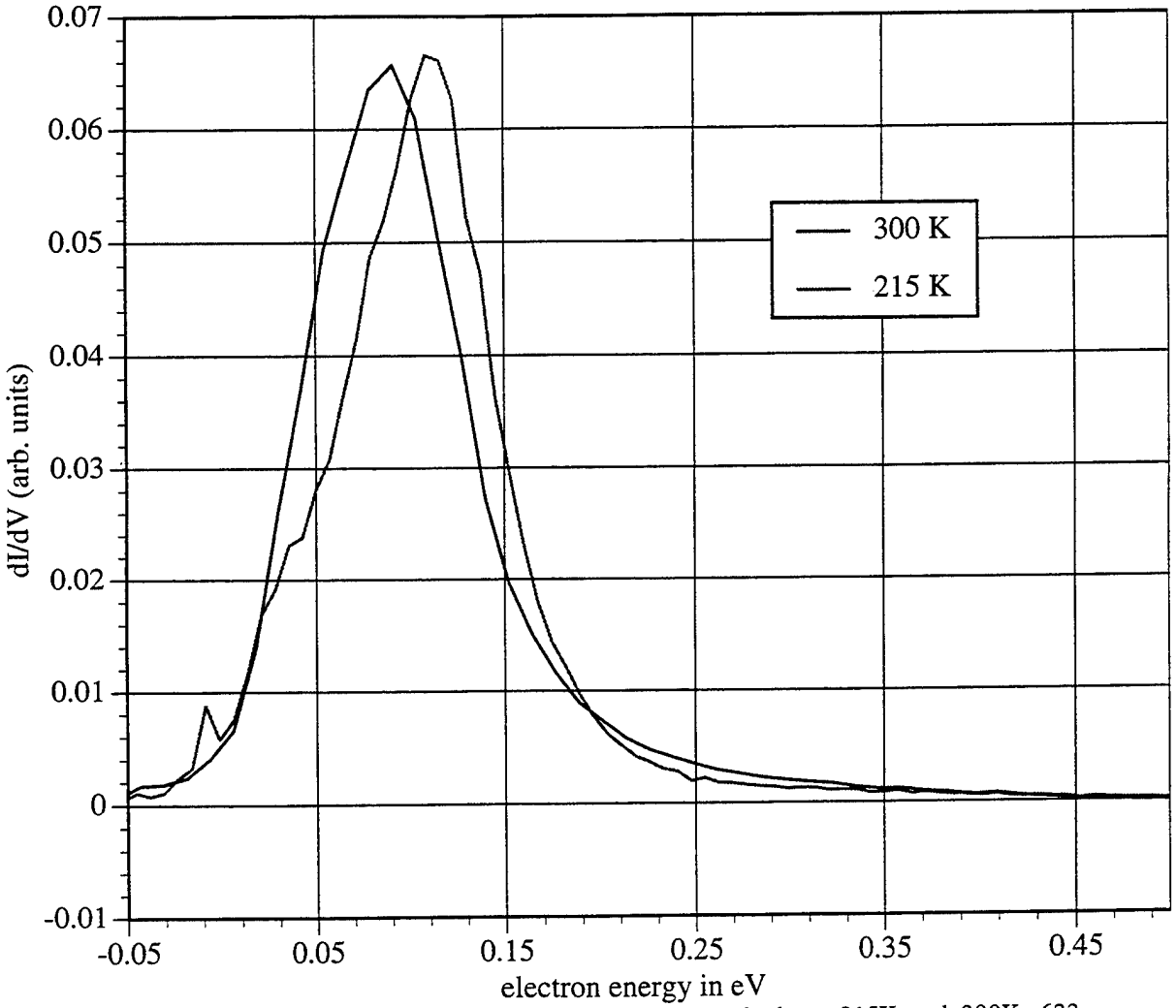

Figure 2. Energy spectra from a 1 micron thick GaAs photocathode at 215K and 300K, 633nm illumination. Electron energies referenced to vacuum level of 215K spectrum.

In addition to the vacuum level cutoff (at zero electron energy, by definition), several other features of the spectra can be seen. The distributions rise to a peak which presumably consists of electrons which thermalized in the bulk and were emitted with minimal energy loss. In this case, these electrons seem to represent a large proportion of the emitted current. Since the thermalized electrons enter the band bending region with a Maxwell-Boltzmann distribution of energies with respect to the bulk CBM, the position of the peak should correspond to the bulk CBM, plus a factor of roughly kT. The 215K peak can be seen to be higher than the 300K peak, due to the increase in band gap at lower temperatures (the Fermi level should not move appreciably with temperature because of the degenerate doping of the semiconductor).

The electrons lower in energy than the peak are those that have escaped after losing some energy to phonon scattering in the cathode. This part of the curve can be seen to be slightly lower in the 215K curve. This fact can be explained by the lower phonon density at 215K.

The spectra immediately above the peak in energy, in the energy range 0.11 - 0.21 eV, are dominated by the high-energy tail of the Maxwell-Boltzmann distribution. This part of the spectra fits well to M-B distributions at the appropriate temperature for both curves. The greater slope of the 215K curve is clearly seen.

The spectra above 0.25 eV are dominated by hot electrons, which are present because of the relative thinness (0.8 microns) of the cathode compared to the absorption depth of 633nm light (approx. 0.3 microns); the active region absorbs only approximately 93% of the light that reaches it, leading to a significant, but small, intensity of light near the photocathode surface. The hot electrons have energies extending at least up to 0.4eV above the spectral peak, which is not surprising considering the photon energy (1.96eV), which can generate electrons with energies of up to 0.54 eV above the bulk CBM.

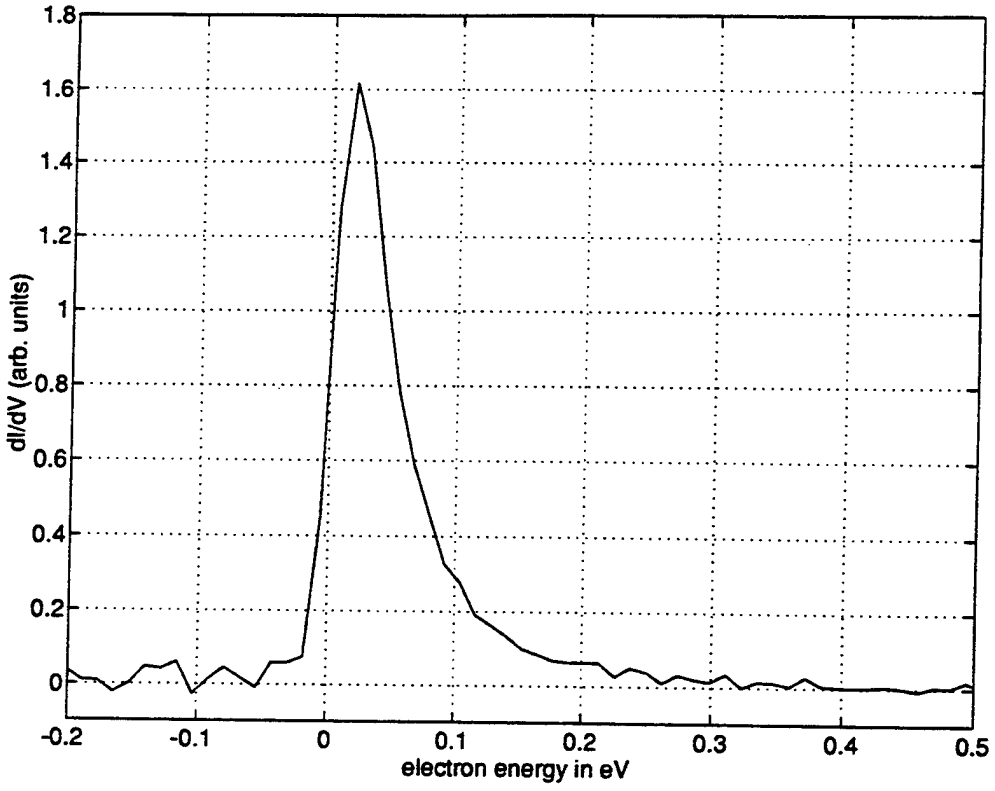

Figure 3. Energy spectrum from same cathode as in figure 2, in an overcesiated condition.

5.2. 0.8 micron thick GaAs photocathode — Spectrum in an overcesiated state

The balance of Cs and O in the activation layer has strong effect on the vacuum level. The energy spectrum of figure 3 is from the same cathode as above, but in an overcesiated state, with the vacuum level approximately 100meV higher. A baking treatment later corrected the stoiciometric balance (and/or altered the structure of the activation layer) and lowered the vacuum level to fully activate the cathode; the figure 2 data were obtained after this treatment. The quantum efficiency for the overcesiated cathode was 2.2% for 633nm illumination.

The crispness and asymmetry of the distribution below attest to the resolution of the parallel-plate retarding technique. The vacuum level cutoff is very sharp, and the only escaping electrons are the high-energy M-B tail and the hot electrons. The FWHM of the distribution is approximately 50meV, the lowest room temperature energy spread ever reported from an NEA photocathode.

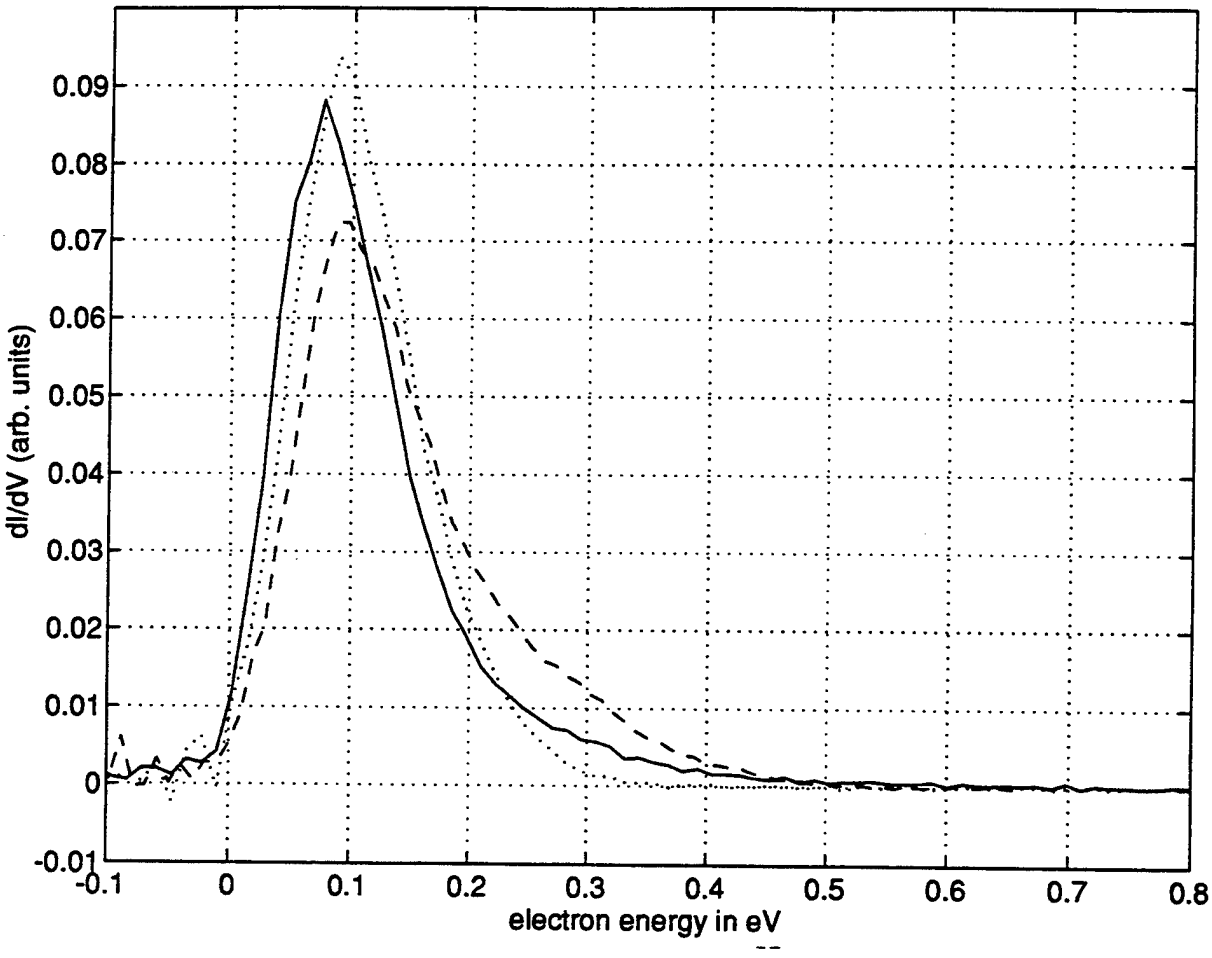

Figure 4.a. Energy spectra from a 0.5 micron thick GaAs photocathode at three different wavelengths — 490nm (dashed line); 650 nm (dash-dot line); and 750 nm (solid line)

5.3. 0.5 micron thick GaAs photocathode — Variations in wavelength, "hot" electrons

Energy spectra were also obtained from a similarly doped and activated GaAs photocathode grown with a 0.5 micron thick active region. In this case the hot electrons can form a significant part of the spectrum, as shown in figures 4.a. and 4.b., where the spectra for 490 nm, 650 nm, and 750 nm light are shown. The curves are scaled to have the same integrated area. Using published absorption coefficients[3] the percent of the light that reaches the front surface of the photocathode, neglecting reflection and all absorption outside of the active region, can be calculated: 3.6% for 490nm, 19% for 650nm, and 60% for 750 nm. Thus the 490 nm spectrum can be taken as a distribution almost entirely derived from electrons thermalized in the bulk, except for a relatively small high energy tail. The vacuum level seems to be somewhat higher than of the cathode discussed above, due to the closeness of the spectral peak to the vacuum level cutoff. The 650 nm spectrum is clearly distorted by the presence of hot electrons at energies significantly above (0.1-0.3V) the peaks of the distributions, which, judging from their "roundness" on the low energy side, are probably close to the CBM and the thermal distribution peak. This roundness is in contrast to the peak of figure 3, which is sharply cut off on the vacuum level side, implying that the peak of the thermal distribution (and thus the CBM) is below the vacuum level. The 750 nm curve is narrower than the 650 nm curve, due to the lower energy of the incident photons, but comparison with the 490 nm data reveals the presence of a significant number of hot electrons. At this wavelength, however, it is difficult to distinguish between electrons emitted "hot" and electrons emitted after thermalizing in the bulk.

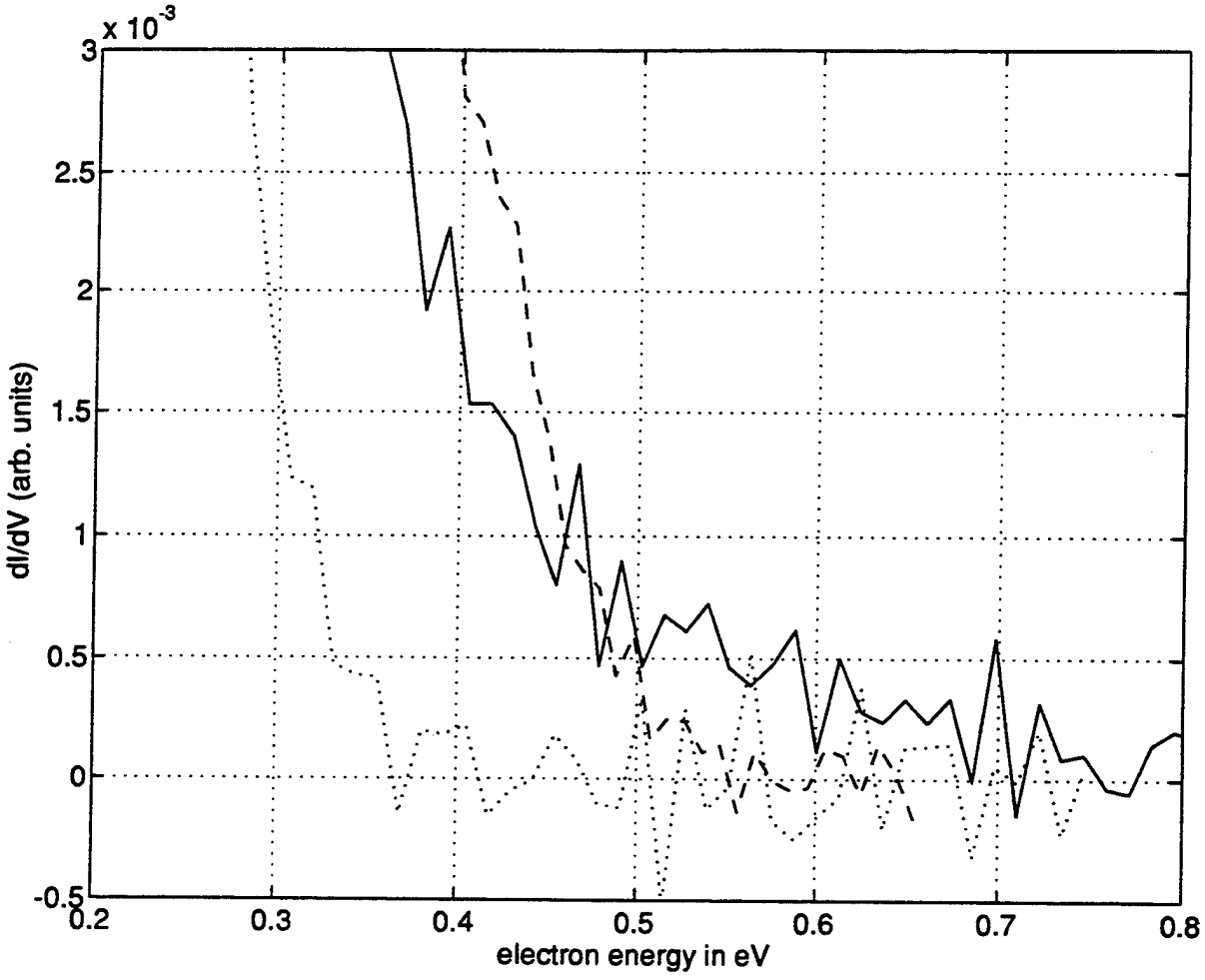

Figure 4.b. Same data, magnified vertical scale to show hot electron distributions

Figure 4.b. magnifies the vertical scale so that the high energy tails (consisting almost entirely of hot electrons) can be seen up to the maximum energy. The highest energy electrons emitted with 750 nm illumination have an energy of approximately 0.36 eV, which is surprising because this represents an energy approximately 0.29 eV above the 490 nm peak, which is likely to be above the bulk CBM; since 750 nm radiation has an energy of 1.65 eV, it should only be able to excite electrons to an energy of ~0.23eV above the CBM, assuming a bandgap of 1.42eV. The higher energy electrons may arise from phonon absorption, or possibly work function variation on the collector or vacuum level variation on the cathode.

The 650 nm distribution cuts off at roughly 0.56eV, 0.49 above the 490 nm curve's peak, corresponding well with the energy of the photons (1.9 eV, translating to a maximum energy of ~0.48 above the vacuum level). The 490 nm distribution has no clear cutoff, which is expected because the 2.52 eV photons can lift an electron 1.1eV above the bulk CBM, well beyond the range of the energy scan.

The energy spectra are seen to be in good agreement with the general picture of energy spectra from GaAs NEA photocathodes, of a vacuum level, a thermal peak corresponding to the bulk CBM with a M-B tail and hot electrons higher in energy. The scattered electron part of the spectrum could not be distinguished because of the slightly higher vacuum level in this case.

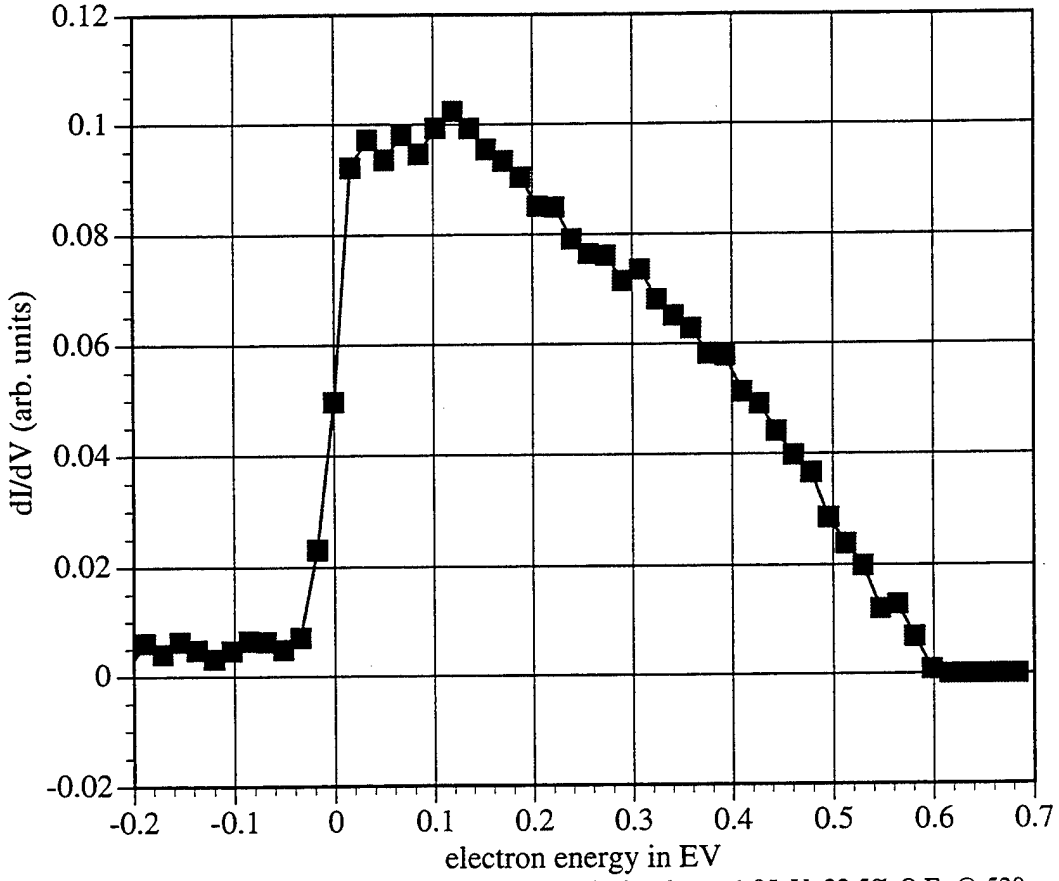

Figure 13. Energy spectrum from GaAsP photocathode, bandgap ~1.85eV, 32.5% Q.E. @ 530nm .

5.4. GaAsP Energy Spectrum

It is interesting to compare GaAs energy spectra to those from a higher bandgap material. The energy spectrum from GaAsP with a bandgap of ~1.85 eV was measured in a very short, simple tube with no specialized electrodes; the collection surface was the phosphor itself, which was ~750 microns above the

surface of the cathode. The cathode had high Q.E. (~1600uA/lm) and was doped to ~5e18. Due to its higher bandgap the GaAsP has much higher NEA (the Cs-O layer lowers the work function to about the same level for both materials), and this results in a much wider energy spectrum, as much-scattered electrons can still escape. However, the amount of scattering taking place seems to be much greater, as the high energy thermal/CBM peak is missing. The increased scattering can be attributed to the wider BB region, caused by increased NEA and lower doping, as well as greatly increased intervalley scattering due to the high-mass X and L valleys being closer to the Γ valley.

SUMMARY

The special tubes described in Part 1 (and one simpler GaAsP tube) were used to measure the energy spectra of a different cathodes at different temperatures, activation layer conditions, and wavelengths. A high resolution spectrum from a fully activated GaAs NEA photocathode can be divided into several pieces, each of which indicates some properties of the photocathode system — the vacuum level cutoff, the scattered electron distribution, the thermal peak, the high-energy Maxwell-Boltzmann tail, and the hot electrons — each of which (except for the vacuum level) may or may not be observable in a given spectrum. This picture was shown to be consistent with the presented spectra. Lowering the temperature of the cathode to 215K narrows the M-B distribution and decreases the number of scattered electrons. The position of the CBM, as seen by the thermal peak, moves upward in energy. The energy spread of the electrons emitted from the GaAs cathodes was typically less than 150meV, with one distribution having a FWHM energy spread of approximately 50meV, the lowest room temperature energy spread from an NEA photocathode ever reported. Hot electrons were seen to be a significant part of the energy spectrum for a 0.5 micron thick GaAs photocathode, and their distribution seemed consistent with the picture of the energy spectrum developed above and known wavelength-dependent absorption coefficients. Data from a GaAsP cathode showed the effects of higher NEA and increased scattering, as the distribution was wider (~0.6 eV), with no evidence of a thermal peak corresponding to the CBM.

This work was supported by the ARPA Advanced Lithography Program under ONR Grant No. N0001492J1996 .

Aaron Baum was supported by an NSF Graduate Fellowship during the period of this work.

---

[1] R.L. Bell, *Negative Electron Affinity Devices*, Clarendon Press, New York, 1973.
[2] A.S. Terekohov and D.A. Orlov, JETP Lett. **59**, 864 (1994).
[3] J.S. Blakemore, J. Applied Phys. **53**, R123-R181 (1982)

IEDM 95

High-Performance Negative Electron Affinity Photocathodes for High Resolution Electron Beam Lithography and Metrology

A. W. Baum, J. E. Schneider, R.F.W. Pease, and W.E. Spicer

Solid State Electronics Laboratory
Stanford University
Stanford, CA

K. A. Costello and V. W. Aebi

Intevac, Inc.
Advanced Technology Division
Santa Clara, CA

Abstract

Factors affecting the brightness of negative electron affinity photocathodes have been investigated experimentally and theoretically. The results of a two-dimensional model of electron dynamics in the cathode, including the effects of surface-trapped electrons, are presented. Emission is seen to be cut off in the central emission area at high current levels. The angular distribution is compared to a cosine distribution based on an energy spectrum obtained from the same cathode. While superior to the cosine distribution with respect to its forward focusing properties, it is far wider than previous theory has suggested.

Introduction

NEAPCs (negative electron affinity photocathodes) have been used for a decade or more in infrared detection equipment as well as in specialty electron guns for high energy physics and magnetic materials analysis. The potential of the NEAPC to be an extremely flexible, high performance electron source for demanding electron beam applications has recently been demonstrated. (1) (2) Energy spreads as small as 50 meV at room temperature have been demonstrated. Moreover, brightnesses of 10^8 A/cm^2-sr at 3kV have been measured; this figure is comparable to that of field emission sources. The diameter of the emission area in this case, 1.7 μm (with the potential for much smaller emission areas), obtained with a single laser beam on an 18 mm diameter cathode, suggests the possibility of massively parallel beam emission using multiple laser beams or patterned illumination. The picosecond-scale switching time of the cathode has already been demonstrated, as well as precision control of emission by modulation of the illuminating light. (3)

The structure and principle of photoemission from a NEAPC is illustrated schematically in Figure 1. The photocathode consists of a semiconductor, usually a III-V compound such as GaAs, heavily p-doped (1-5x10^{19} cm^{-3}) so as to raise the conduction band relative to the Fermi level. The clean semiconductor surface is coated with a layer of Cs and O a few monolayers thick. This activation layer lowers the work function so that the conduction band in the bulk is above the vacuum level, a condition of negative electron affinity. If electrons are excited into the conduction band within a diffusion length (typically a few μm) of the surface, many of them will diffuse to the surface where they will have a high probability of escaping into vacuum. (4) (5) The work described below was performed on cathodes sealed in modified night vision tubes. Their structure has been discussed elsewhere. (1)

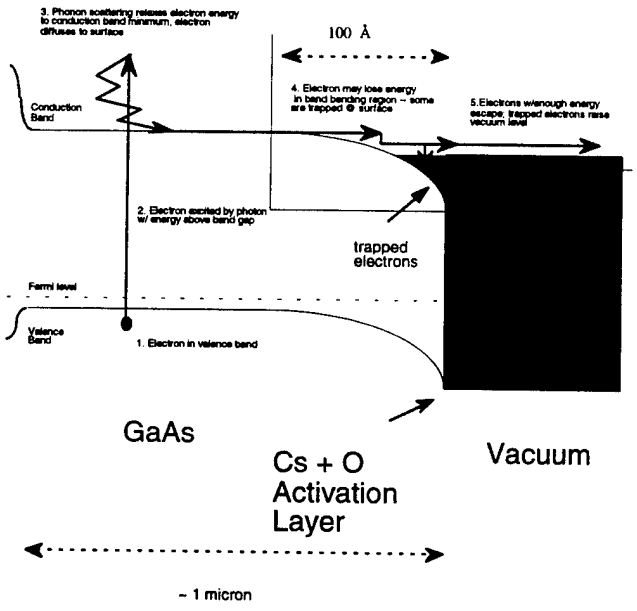

Figure 1: Band diagram of NEAPC, with schematic depiction of emission process.

The mechanisms determining brightness in NEAPCs have not previously been investigated in detail. This fact, combined with the importance of brightness in electron beam systems, motivated this work. Cathode brightness is governed both by the current density at the cathode surface and by the angular distribution of the emitted electrons. As these two factors are controlled by different mechanisms, they will be discussed separately.

Brightness: Measurements and Modeling of Surface Effects

The ability of NEAPCs to emit electrons is determined by the position of the vacuum level. The cutting-off of electron emission by movement of the vacuum level is illustrated in Figure 2, which shows energy spectra (dI/dV curves) from a GaAs cathode undergoing successive bakes to improve the activation. The basic structure of energy spectra from NEAPCs is discussed elsewhere. (2)

If an electron reaches the surface with energy less than the vacuum level, it cannot escape. Since the electrons reach the surface with a range of energies, changes in the vacuum level alter the probability that an electron reaching the surface will escape into vacuum.

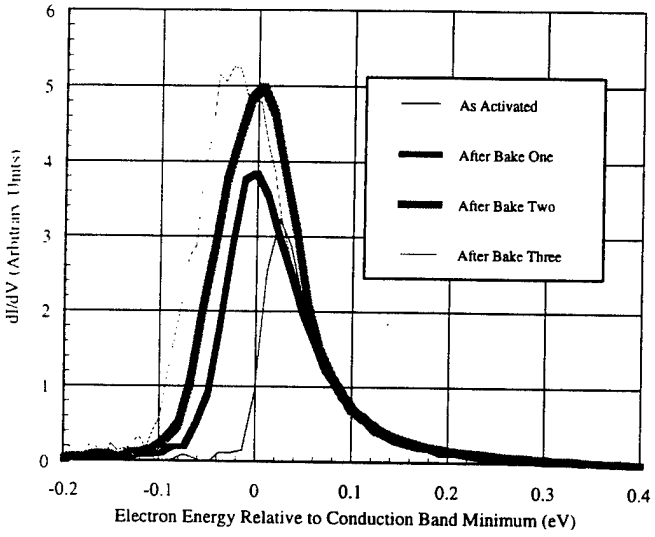

Figure 2: Energy spectra for GaAs photocathode after successive bakes, showing movement of vacuum level.

Electrons which lose too much energy to escape are trapped at the surface of the cathode until they can recombine with holes in the bulk. If the current density is high, the charge of these trapped electrons can raise the vacuum level relative to the bulk, cutting off emission. These electrons eventually recombine with holes tunneling through the depletion region. However, the trapped electrons will diffuse laterally in the surface layer especially if the emission area is small. This action reduces their sheet density, and thus reduces their impact on the vacuum level. The lateral electric field produced by their charge will also promote lateral movement. Based on this reasoning, the current density from a micron-scale emission spots has been investigated and found to be approximately two orders of magnitude higher than previous measurements which had used spot sizes generally larger than 100 μm.

To investigate this effect further a computer simulation of the interaction between trapped and emitted electrons has been created. The simulation program consists of three modules: a simulation of the electrons in the bulk, a simulation of the trapped electrons, and a master program that controls iteration between the two modules until they agree to within a specified accuracy.

The first simulation is a model of the excitation of electrons into the conduction band by an incident light beam and their subsequent diffusion. Due to the rotational symmetry of the problem, only 2 dimensions are needed: radial (r) and depth (z). The excitation beam, consisting of 633 nm light, has a gaussian distribution in the r direction, with an exponential decline toward the surface. The module obtained the steady-state distribution of conduction-band electrons by directly simulating the diffusion of the electrons from an initial distribution using the given excitation, ordinary bulk diffusion, and certain boundary conditions. On the back face of the GaAs active region, the AlGaAs interface, diffusion is assumed to be zero. For radial distances greater than twenty times the nominal (gaussian) radius of the illuminated spot, the electron density is set at zero. The effective recombination velocity on the CsO/vacuum interface varies with radius due to the presence of the surface-trapped electrons. On the first iteration, the recombination velocity is determined by an initial guess; on subsequent iterations, the values are passed from the second module.

The second module determined the 1-dimensional distribution of surface charge density. Once again the diffusion equations, in this case the equations for one-dimensional radial diffusion, were used. The generation rate in each annulus was determined by the density of bulk electrons near the surface, $n_{bs}(r)$, as calculated by the first module. The electrons were assumed to diffuse into the surface region with thermal velocities, $v_T = (kT/m)^{1/2}$, with all of these electrons either escaping into vacuum, returning to the bulk, or becoming trapped and later recombining. A fixed fraction, $0.6 \cdot v_T \cdot n_{bs}(r)$, were assumed to become trapped. The fraction escaping into vacuum was determined by the expression

$$0.4 \cdot v_T \cdot n_{bs}(r) \cdot (NEA - q \cdot x_{BB} \cdot n_s(r) / \varepsilon_s) / NEA, \quad (1)$$

where x_{BB} is the band-bending region width, $n_s(r)$ is the local surface charge density, and NEA is the initial value of the cathode NEA. The effective recombination velocity used for the bulk calculations is the total of these two. Recombination of the trapped electrons is assumed to follow an exponential dependence on the movement of the vacuum level, in the same manner as thermionic emission, which is thought to be the main route of recombination for trapped electrons in most cathodes. The recombination rate is defined for a vacuum level raised by 0.1V.

The physical parameters used in the simulation are shown in Table 1; they are meant to replicate the conditions under which the high brightness results have been obtained previously. While many of them are accepted approximate values, two surface parameters are rather crude estimates. The mobility of the electrons on the surface is projected to be two orders of magnitude lower than the bulk mobility, with the doping having only a very small effect. (6) The rate of recombination of the electrons is estimated from data obtained by Herrera-Gomez in observing the behavior of nanosecond-scale pulses from GaAs NEAPCs. (7)

The results obtained using these parameters are shown in Figure 3. For 18.5 μA of emission current, the emission area is mainly determined by the spreading of the electrons as they diffuse to the surface; for the higher current levels, emission decreases and is finally blocked off in the center. The maximum current density at the center is reached between 18.9 and 43.5 μA, and on-axis brightness actually decreases with increasing current above this level. This paradoxial behavior is easily understood in terms of the behavior of the trapped electrons, which have the greatest concentration at the center; they thus tend to block emission from the center first. The electrons are then forced to diffuse further from the center to be emitted.

Parameter	*Value*
Temperature	300 K
Initial NEA	0.2 eV
Cathode thickness	1.5 microns
Light spot (diameter)	0.7 microns
x_{BB}	10 nm
Recombination rate at 0.1V	10^9 sec^{-1}
Conduction electron lifetime	2 nsec
Bulk electron mobility	500 cm^2/V-sec
Surface electron mobility	80 cm^2/V-sec

Table 1. Parameters used for the cathode simulation.

The results of the simulation indicate a somewhat larger diameter of emission than was observed; it is possible that the actual cathode's thickness was somewhat less than its nominal value, as it is difficult to measure this in the tube. The current density seems to be limited to approximately 300 A/cm^2, somewhat less than the 841 A/cm^2 previously calculated (1), but within the correct order of magnitude, which is the best that can be expected given the level of accuracy of the parameters.

It has not yet been possible to observe the dependency of the shape and size of the emission area on current at such high current densities. A demountable UHV NEAPC-based electron gun and a beam analysis chamber are currently being constructed to measure these and other important properties of high brightness NEAPC emission.

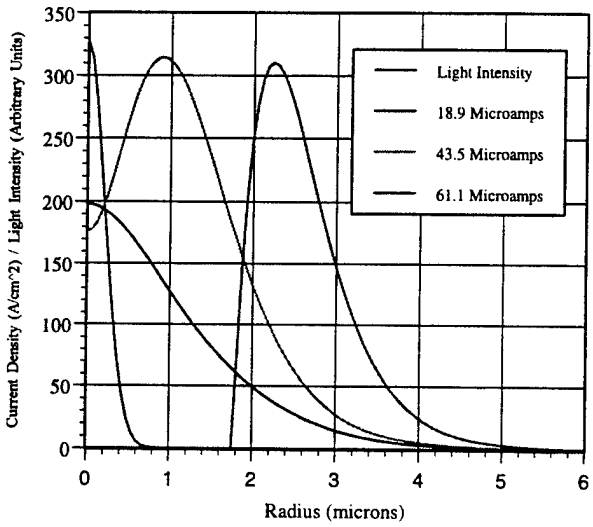

Figure 3: Light intensity versus radius and simulation results showing current density versus radius for three emission levels. Note the spread of electrons from light spot due to bulk diffusion and the cut off at center for high current.

Angular Spread

When the electrons enter the surface band-bending region, the energy of their motion in the lateral direction (parallel to the surface) is of the order of kT. The fields in the band-bending region accelerate the electrons toward the surface, presumably lending them momentum only in the surface normal direction. When the electrons are released from the solid they undergo a change in quantum-mechanical wavelength due to the difference between their effective mass in the GaAs (0.067 m_e), and their mass in vacuum (m_e). For a perfect interface this change of wavelength should lead to a quantum-mechanical refraction analogous to Snell's law which focuses the electrons toward the surface normal, reducing the energy of their lateral motion by a factor equal to the ratio of the semiconductor and vacuum effective masses. These ideas have led several workers to predict extremely low lateral energies for electrons emitted from NEA cathodes. (8) However, in practice much larger angular spreads have been observed. (9)

To gauge the degree of forward-focusing of the electrons emitted from a GaAs NEAPC, the energy spectrum and angular spread have been measured on the same cathode. The energy spectrum shown in Fig. 5 was obtained by the parallel-plate approach described elsewhere. (2) A theoretical angular distribution was calculated based on this energy spectrum, assuming that all of the electrons were emitted in a cosine distribution, *i.e.* in the manner of a perfect Lambertian emitter. Figure 6 compares this calculated distribution to the actual distribution measured from a phosphor image by a technique detailed previously. (1) The cathode was 0.5 micron-thick GaAs doped to ~10^{19} cm^{-3}, activated with Cs and O.

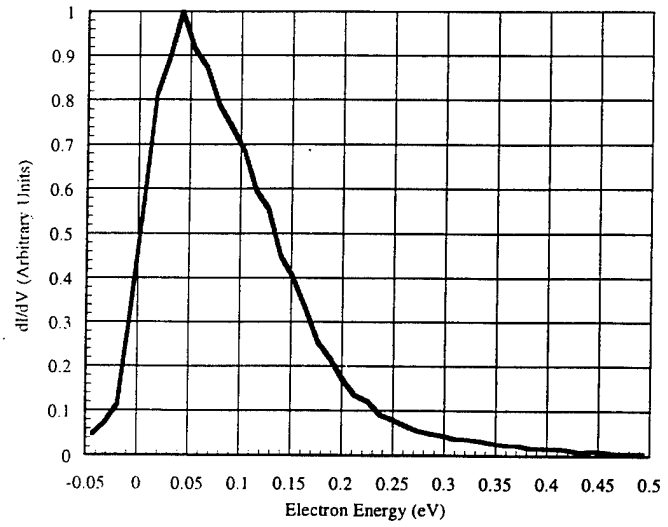

Figure 4: Energy spectrum used to derive cosine angular distribution. Only electron energies greater than zero are used.

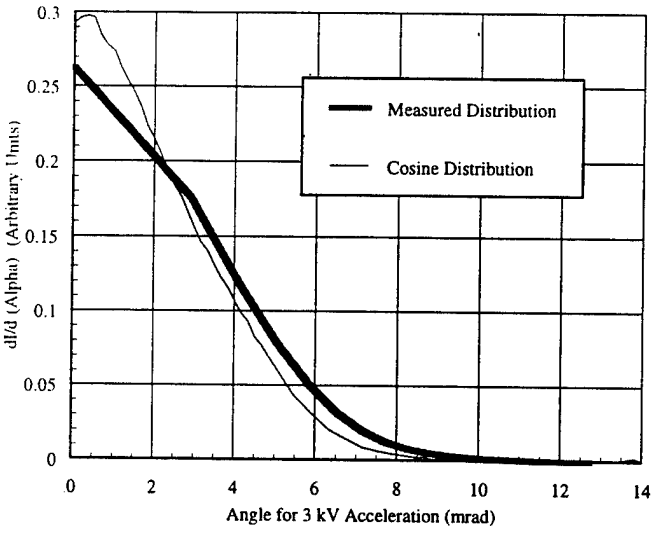

Figure 5: Angular distribution from GaAs NEAPC compared with cosine distribution calculated from energy spectrum of Figure 4.

Clearly, the actual emitted electrons are considerably more forward-focused than the cosine distribution; however, the spread is much larger than previous theory has predicted. Previous workers have tried to explain the width of the angular spread in terms of micropitting, which presumably occurs during the heat cleaning process. (10) Micropitting could play a role on some cathodes, but in this case micropitting can almost certainly be ruled out because cathodes which have gone through similar processing have been found to be flat on a nanometer scale.[11] Other sources of deviation from the idealized model are the nonuniform distribution of dopant atoms in the band-bending region, irregularities in the GaAs/CsO interface, and scattering in the CsO layer. The combined effects of these, and possibly some other mechanisms widen the angular spread far beyond that predicted by simple theoretical models.

Conclusion

However, the fundamental factors influencing brightness of NEAPCs have not been fully investigated. A computer simulation has been created which models the interaction of surface trapped electron with bulk and emitted electrons. Profound changes in emission area size and shape are observed at high current levels. Angular spread measurements have been compared with a theoretical angular distribution generated using a Lambertian model and an experimental energy spectrum from the same cathode. Many questions have been raised by this work which will be addressed using a flexible ultra-high vacuum analysis system which is under construction.

Acknowledgements

The authors would like to acknowledge many useful discussions with Professor William E. Spicer of Stanford, as well as Ken A. Costello and Verle W. Aebi of Intevac, Inc. This work has been supported by the ARPA Advanced Lithography Program under ONR Grant #N0001492J1996. A. W. Baum and J. E. Schneider have been supported by NSF Graduate Fellowships during the period of this work.

References

(1) A. W. Baum, W. E. Spicer, R. F. W. Pease, K. A. Costello, and V. W. Aebi, "Negative electron affinity photocathodes as high performance electron sources - Part 1: Achievement of ultra-high brightness from an NEA photocathode," *Proceedings of the 1995 SPIE International Symposium on Optical Science, Engineering, and Instrumentation (in press).*

(2) A. W. Baum, W. E. Spicer, R. F. W. Pease, K. A. Costello, and V. W. Aebi, "Negative electron affinity photocathodes as high performance electron sources - Part 2: Energy spectrum measurements," *Proceedings of the 1995 SPIE International Symposium on Optical Science, Engineering, and Instrumentation (in press).*

(3) C. A. Sanford, Doctoral Thesis, Cornell University, 1990.

(4) W. E. Spicer, Phys. Rev. **112** (1958), 114.

(5) C. N. Berglund and W. E. Spicer, Phys. Rev. **136** (1964) A1030-A1044.
(6) Zhiping Yu, private communication, 1995.
(7) A. Herrera-Gomez and W. E. Spicer, "Physics of High Intensity Nanosecond Electron Source," *Proceedings of the 1993 SPIE International Symposium on Optical Science, Engineering, and Instrumentation,* **2022** (1993), 51-63.
(8) R.L. Bell, *Negative Electron Affinity Devices,* Oxford: Clarendon Press, 1972.
(9) D. C. Rodway and M. B. Allenson, J. Phys. D: Appl. Phys. **19** (1986), 1353-1371.
(10) D. J. Bradley, M. B. Allenson, and B. R.Holeman, J. Phys. D: Appl. Phys. **10** (1977), 111-125.
(11) Verle Aebi, private communications, 1994.

Semiconductor on glass photocathodes as high-performance sources for parallel electron beam lithography

J. E. Schneider,[a] A. W. Baum, G. I. Winograd, R. F. W. Pease, M. McCord, and W. E. Spicer
Solid State Electronics Laboratory, Stanford University, Stanford, California 94305-4075

K. A. Costello and V. W. Aebi
Intevac, Inc. Advanced Technologies Division, Santa Clara, California 95054

(Received 30 May 1996; accepted 17 August 1996)

The throughput of electron beam lithography has historically been limited by electron–electron interactions that cause blurring at high currents. We present a system configuration for maskless parallel electron beam lithography using a new multiple primary source technology that, by employing widely spaced beams, significantly reduces this problem. The proposed source technology, a negative electron affinity (NEA) photocathode, allows us to generate an array of high brightness, low energy spread, independently modulated beams over a large area. In order to assess the effects of electron–electron interactions in this system, Monte Carlo simulations have been performed. The results of these calculations indicate that this configuration enjoys significant advantages over existing maskless systems. By restricting the area of emission for the individual beamlets to submicron dimensions, the blurring due to statistical electron–electron interactions can be significantly reduced for a given current at the wafer. For example, at 50 kV a total current of more than 2.5 μA can be obtained with less than 10 nm beam blurring. Preliminary experimental results suggest that high brightness emission can be maintained from a NEA photocathode in a demountable vacuum system.

I. INTRODUCTION

One subject of intense research in recent years has been the possibility of increasing the throughput of electron beam direct write technology to be competitive for wafer production for linewidths of 0.1 μm and below. It has been recognized that the most straightforward way of achieving higher throughput direct write equipment is to dramatically increase the current in the electron beam column (without increasing the landing energy). Several prototype systems have been proposed which rely on the generation of an extended, high-current (several microamps) exposing beam for electron or ion image projection.[1–5] Other proposed systems have included the use of a large array of secondary sources or blanking apertures following a wide-area, collimated beam.[6,7] It has been suggested, however, that by using multiple primary sources, useful throughput may be achieved for total currents at the wafer between 0.5 and a few microamps.[8] Here we propose a new system configuration in which multiplexed primary sources illuminate the wafer through the use of a simple, two lens demagnifying projection system. Because the system employs an array of independently modulated Gaussian beams, a raster scan system can be used that has the advantage of being maskless. The centerpiece of this configuration is a new parallel electron source technology currently under development in our laboratory.

The proposed source, a negative electron affinity (NEA) photocathode, has thus far been used in high efficiency image intensifiers for night vision applications, as well as in specialty electron sources for experimental particle physics. Recently, however, Baum *et al.* demonstrated excellent source properties experimentally in specially modified night vision tubes.[9,10] Beam brightnesses of 1×10^8 A/(cm^2 sr) from a 1.7 μm diameter illuminating spot, as well as energy spreads of 50–200 meV, have been measured. In addition to these properties, NEA photocathodes also exhibit highly uniform emission to within 5% over a large area (100 mm^2), and have picosecond-scale switching times.[11] Moreover, since these cathodes are fabricated from GaAs, they may be excited with visible red diode lasers at 635 nm. These diode lasers have the advantages that they may be modulated at gigahertz rates, and are available in an off-the-shelf array format. The cathodes themselves may also be easily customized using band gap engineering and lithography techniques developed for technologically mature III–V materials systems.

For many years, the importance of electron–electron interactions in moderate to high-current probe forming systems has been known.[12,13] These interactions produce three basic effects which are pertinent to system design. Stochastic interactions between electrons can cause broadening of the energy distribution of electrons in the beam; this phenomenon is known as the Boersch effect. Stochastic interactions also give rise to the trajectory displacement effect, which leads to a blurring of the final probe beam diameter at the image plane. The global space charge effect in the beam gives rise to defocusing and can generally be corrected for by controlling lens strength. Because the Boersch and trajectory displacement effects cannot be corrected for, they are of primary concern to us in this study. There has been a body of work on the simulation of these effects in electron beam

[a]Electronic mail: jims@jump.stanford.edu

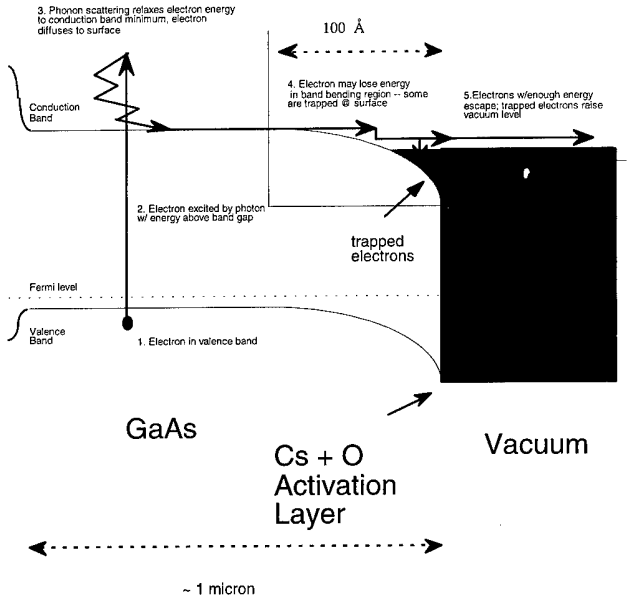

FIG. 1. Band diagram of a NEA photocathode with a schematic of the photoemission process.

instruments, including two programs commercially available for this purpose.[14,15] We have developed a simulator which is optimized for the modeling of multiplexed primary and secondary sources, and for large numbers of electrons. In this article, we present an analysis of electron–electron interaction effects in a proposed NEA photocathode-based parallel electron beam direct write system.

II. THE PHYSICS OF NEGATIVE ELECTRON AFFINITY

The structure and principle of photoemission from an NEA photocathode is illustrated schematically in Fig. 1. The photocathode consists of a semiconductor, usually a III–V compound such as GaAs, epitaxially grown on top of a diffusion blocking layer. This structure is bonded to a glass substrate, which has a antireflection coating on one side. The substrate provides the mechanical rigidity necessary to ensure the physical ruggedness of the overall cathode structure. The semiconductor layer itself is heavily p-doped ($1–5\times10^{19}$ cm^{-3}) so as to raise the conduction band relative to the Fermi level. The clean semiconductor surface is coated with a layer of Cs and O a few monolayers thick. The activation layer lowers the work function so that the conduction band in the bulk is above the vacuum level, a condition of negative electron affinity. If electrons are excited into the conduction band within a diffusion length (typically a few microns) of the surface, many of them will diffuse to the surface where they will have a high probability of escaping into the vacuum.[16,17] The electrons in a transmission mode photocathode may are excited using a red visible laser at approximately 635 nm, which is focused through the glass substrate onto the thin (~1 μm) semiconductor bulk region. A diffraction-limited illuminating laser spot can be made as small as 0.5 μm, and the emitted electrons will have a

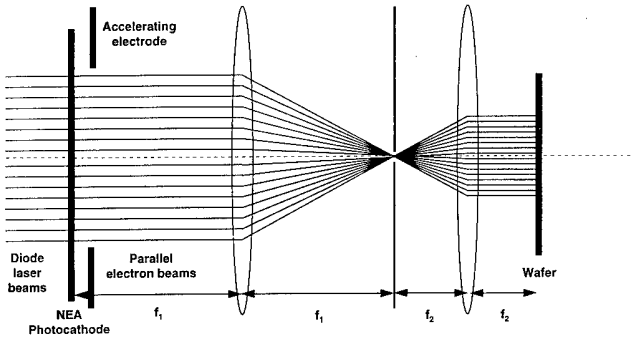

FIG. 2. Simulated parallel electron beam lithography system configuration based on a negative electron affinity photocathode. Divergence due to the accelerating electrode can be compensated by an auxiliary magnetic lens and is absent. The lens are all represented as thin lenses.

Gaussian spatial distribution of comparable dimensions. These emitted electrons may then be focused using electron optics on the opposite side of the photocathode surface.

III. SIMULATION OF COULOMB INTERACTIONS

A. Electron optical test system and spot size

Patterning 100 nm features in manufacturing requires the beam diameter to be no more than 30–40 nm to maintain linewidth control. The proposed design uses two lenses to demagnify an electron source of diameter of 0.5 μm by a factor of 15 (Fig. 2). The minimum beam diameter as a function of the convergence angle at the image may be approximated by the quadrature sum of the beam diameters due to each component. The contributions of spherical aberration, chromatic aberration, diffraction, and demagnification to the minimum beam diameter are shown in Fig. 3 for the values of C_s, C_c, and ΔV shown. It is clear from inspection of Fig. 3 that the maximum attainable convergence angle at the wafer without significant spherical aberration is approximately 10 mrad corresponding to an acceptance angle at the source of 0.67 mrad. For a 50 kV beam and a uniformly distributed

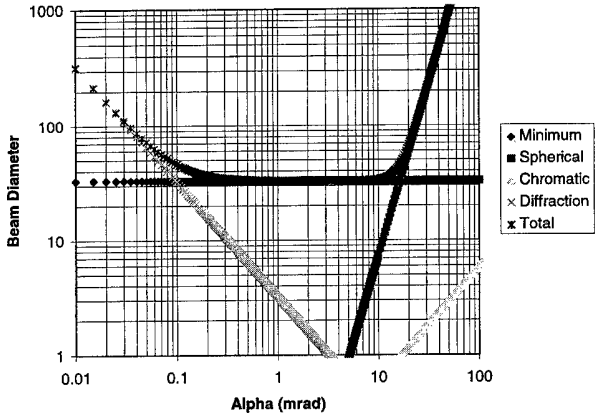

FIG. 3. The effects of aberrations on beam diameter in the proposed system. The system parameters used are f_2 = 15 mm, C_S = 18 mm, C_C =15 mm, ΔV=0.2 eV, and V=50 kV.

energy spread at the source of 0.2 eV, the total source divergence is 2 mrad. Taking into account the cosine distribution of the electrons at the source, this corresponds to a current efficiency of 36% (i.e., 36% of the emitted current reaches the target).

If the diameter of the source were reduced, less demagnification would be required for a given resolution and this would yield greater current efficiency. To this end, a similar system with 0.1 μm source diameter and lens focal lengths f_1=60 mm and f_2=15 mm was also simulated. These parameters lead to a demagnification of four with a convergence angle at the image of 8 mrad, which corresponds to a maximum convergence angle at the cathode of 2 mrad and a current efficiency approaching 100% for a 240 μm diameter aperture.

B. Monte Carlo simulation of electron–electron interactions

Electron–electron interactions may be simulated as a function of column parameters through a relatively straightforward Monte Carlo simulation process. As a significant amount of work on this subject has been performed and documented elsewhere, we shall describe only the essentials of the simulation below. The monograph by Jansen[14] provides an excellent detailed description of this type of calculation. The overall strategy is first to set the initial conditions of electrons at the source using a random number generator to fit the angular and energy distributions of the emitted electrons to specified parameters. Each electron is emitted randomly within an interval of time determined by the source emission current. In each case, the energy distribution of the electrons is taken to be uniform. While this source model may not be wholly accurate, the descriptions of the velocity and angular distributions as a Gaussian and a cosine distribution are consistent with our earlier experimental observations for NEA photocathodes in sealed tubes.[9,10] In fact, previous angular distribution measurements indicate that a slight forward focusing occurs for an NEA photocathode; thus, taking the distribution to be a cosine represents a conservative estimate.

After emission from the cathode, the electrons are accelerated through a 5 mm field region to 50 kV. There is a diverging lens action at the accelerating electrode which, if necessary, can be compensated by a magnetic lens; this is neglected in our simulations. They are then focused through the objective lens, after which they may be intercepted by the aperture. Finally, the electrons are focused by the projector lens onto the wafer. The convergence angle is chosen so that lens aberrations are negligible. To isolate the effects due to electron–electron interactions, the aberration coefficients are set to zero. After the entire sample of electrons has been simulated, a data collection routine finds the plane of best focus by calculating the point at which the minimum $FW_{0.5}$ image blurring occurs.

To achieve acceptable statistics, the number of particles was chosen such that an increase in the sample size did not affect the calculated results for beam blurring and deflection.

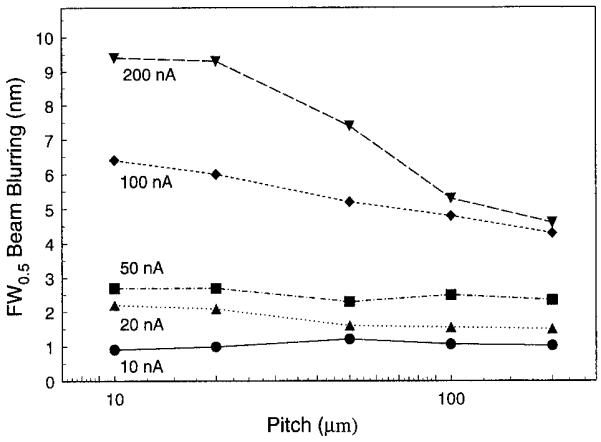

FIG. 4. $FW_{0.5}$ beam blurring vs beamlet pitch for several beamlet currents. The data in each case represent the mean beam blurring in a four beam (2×2) system, with each beam carrying the indicated current.

For example, where 10 nA beamlet currents were used, at least 200 particles per beamlet were simulated; the number of particles used for higher beamlet currents was proportional to the beamlet current as consistent with the above rule. For the most part, the beam statistics are quoted in terms of their $FW_{0.5}$ values, which refer to the widths of the distributions under which 50% of the particles fall. This statistic has been used widely in the literature because it is relatively insensitive to large deflections generated by very small numbers of events, such as the large deflections encountered in near misses between interacting electrons. In the parallel beam simulations, the statistics quoted are averages over the total number of beamlets.

C. Results

For an array of 2×2 beams the final beam properties due to the beamlet current and the pitch (spacing) of beamlets at the source are shown in Fig. 4. For beamlet currents of up to 50 nA, the beam blurring (FWHM) is relatively insensitive to pitch; as the beamlet current is further increased the blurring becomes significant. For a beamlet current of 200 nA, the blurring is 9 nm for a pitch of 10 μm, compared with 4 nm for a 200 μm pitch. A similar trend may be seen in the values for the $FW_{0.5}$ energy broadening (Boersch effect), shown in Fig. 5.

To estimate how the previous results scale with higher total currents, a small individual beamlet current (10 nA) with correspondingly small blurring was taken as the base case, and the number of beams was increased. Two configurations, one with a 0.5 μm source diameter and one with a 0.1 μm source diameter, were analyzed in terms of the blurring of the final image as a function of the total target current and the number of beams needed to achieve that current (Fig. 6). With 0.5 μm diameter sources, as can be obtained by focusing the incident laser light to a diffraction-limited spot, it appears that a beam current of 0.5 μA can be obtained before beam blurring reaches 10 nm. This is achieved with an array of 144 (12×12) beamlets on a 50 μm pitch. By

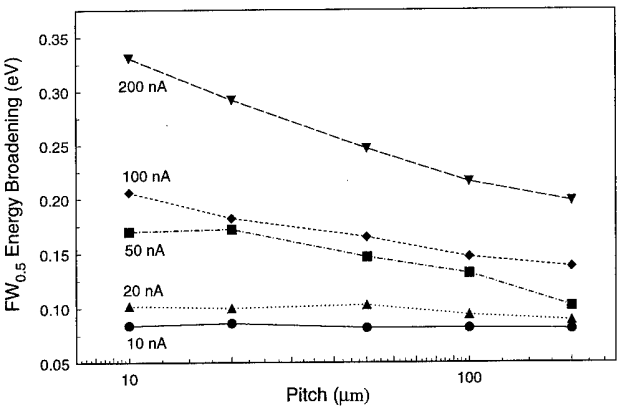

FIG. 5. $FW_{0.5}$ energy broadening vs beamlet pitch for several beamlet currents. The data in each case represent the mean beam blurring in a four beam (2×2) system, with each beam carrying the indicated current.

using beamlet sources of 0.1 μm diameter, we can achieve over 2.5 μA before the blurring reaches 10 nm. Thus, there are significant advantages to using smaller sources, which may be achieved by restricting the emission area on the cathode surface.

Spurious deflection of a beamlet due to neighboring beamlets is obviously a concern. While the beam deflection does increase with current as a result of the global space charge effect, the worst-case deflection for 256 beams (50 μm pitch) at a total current of 2.5 μA was 4 nm, less than half the beam blurring.

IV. DISCUSSION AND FUTURE WORK

Realizing a practical system is the obvious goal. To this end we have a number of tasks:

(1) Continued modeling of different column configurations: This includes an analysis of the effects of the accelerating electrode, thick lenses, and off-axis aberrations. One advantage of this configuration is that we can trade off-axis aberrations for space charge effects by adjusting beamlet pitch. For the cases we have considered here the off-axis aberrations should not limit the field of view. For example, 16×16 sources on a 50 μm pitch represent a field size of 800 μm at the object and only 200 μm at the wafer; Munro *et al.* indicated that immersion lenses (such as that used in the accelerating region) enjoy even lower aberrations than do conventional lenses.[18]

(2) Experimental verification: Currently under construction in our laboratory is an ultrahigh vacuum (UHV) facility designed for the activation and testing of NEA photocathodes. The first part of the system consists of a chamber designed for cathode activations with Cs and O. This chamber may be used to test the spectral photoresponse of the cathodes, as well as to test novel activation procedures. The second portion of the facility is a specially designed electron gun, in which various cathodes may be inserted, evaluated, and replaced under vacuum. This electron gun incorporates specialized electron optics designed to provide an optimal UHV environment for the cathode, since the cathode is sensitive to surface contamination. The third and final portion of the system is a versatile UHV electron optics column and chamber in which the emitted beam properties may be analyzed. Moreover, this chamber will serve as a test bed for the study of long-term stability and lifetime of the cathode source, during which time the effects of various materials typically found in semiconductor processing environments on cathode performance will be assessed. To date, both the activation and beam analysis chambers have been completed. A cathode has been successfully activated to a state of negative electron affinity with 22% quantum efficiency at 633 nm, and has been operated at 6 μA for a period of time over 10 h with no indications of decay during preliminary stability and drift tests. The electron gun is currently being assembled, and will be tested soon after its completion.

(3) Realization of 0.1 μm source: With our existing cathode, the source diameter is minimized to 0.5 μm by focusing the laser illumination to a diffraction limited spot. Smaller sources will require a different approach, such as patterning the cathode to restrict the area of NEA to 0.1 μm while retaining high brightness.

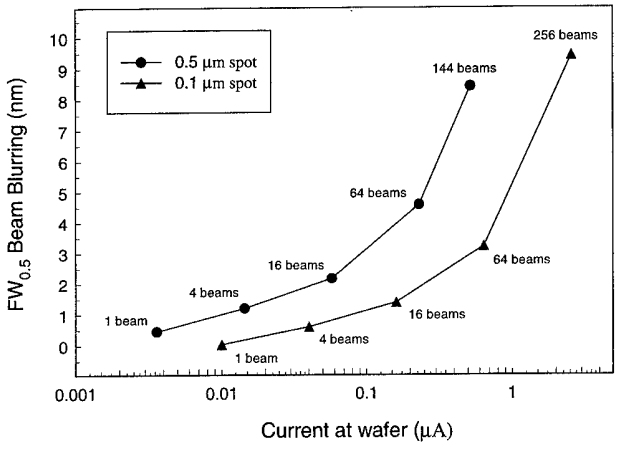

FIG. 6. $FW_{0.5}$ beam blurring vs the number of beams and total current at the wafer for both patterned and unpatterned cathodes. For a given system resolution, the patterned cathode requires less demagnification and requires approximately three times less current. Thus, for a given throughput, the use of a patterned cathode results in significantly less beam blurring.

V. CONCLUSIONS

We have proposed a simple demagnifying system architecture for high-throughput electron beam lithography which relies on a high-performance negative electron affinity photocathode source. Cathodes with different source diameters have been simulated, and resultant beam blurring and energy broadening for each system has been calculated for sources with different pitches and beamlet currents. The benefits of the high-brightness, low energy spread NEA source have been demonstrated with respect to both current efficiency and beam blurring. For the systems tested, electron–electron interactions do not appear to be limiting factor for a 0.1 μm system resolution and up to 2.5 μA at 50 kV.

ACKNOWLEDGMENTS

This work has been supported by the ARPA Advanced Lithography Program under ONR Grant No. N0001492J1996. J. E. Schneider has been supported by a NSF Graduate Fellowship during the period of this work.

[1]S. D. Berger and J. M. Gibson, Appl. Phys. Lett. **57**, 153 (1990).
[2]G. Stengl *et al.*, J. Vac. Sci. Technol. B **9**, 2824 (1992).
[3]M. B. Heritage, J. Vac. Sci. Technol. **12**, 1135 (1975).
[4]J. Frosien, B. Lischke, and K. Anger, J. Vac. Sci. Technol. **16**, 1827 (1980).
[5]W. H. Brunger, M. Torkler, and L. M. Buchman, J. Vac. Sci. Technol. B **10**, 2829 (1992).
[6]T. H. Newman, R. F. W. Pease, and W. Devore, J. Vac. Sci. Technol. B **1**, 999 (1983).
[7]Yasuda *et al.*, Jpn. J. Appl. Phys. **32**, 6012 (1993).
[8]C. N. Berglund (private communication).
[9]A. W. Baum, W. E. Spicer, R. F. W. Pease, K. A. Costello, and V. W. Aebi, *Proceedings of the 1995 SPIE International Symposium on Optical Science, Engineering, and Instrumentation* (SPIE, Bellingham, WA), Vol. 2522, p. 208.
[10]A. W. Baum, W. E. Spicer, R. F. W. Pease, K. A. Costello, and V. W. Aebi, *Proceedings of the 1995 SPIE International Symposium on Optical Science, Engineering, and Instrumentation* (SPIE, Bellingham, WA), Vol. 2550, p. 189.
[11]C. A. Sanford, Doctoral thesis, Cornell University, 1990.
[12]A. N. Broers and H. C. Pfeiffer, Proceedings of the 11th Symposium on Electron, Ion and Laser Beam Technology, San Francisco, 1971 (unpublished).
[13]H. C. Pfeiffer, Proceedings of the 5th Symposium on Scanning Electron Microscopy, Chicago, 1972 (unpublished), p. 113.
[14]G. H. Jansen, *Coulomb Interactions in Particle Beams* (Academic, New York, 1990).
[15]E. Munro, Nucl. Instrum. Methods Phys. Res. A **258**, 443 (1987).
[16]W. E. Spicer, Phys. Rev. **112** (1958), 114.
[17]C. N. Berglund and W. E. Spicer, Phys. Rev. **136**, A1030 (1964).
[18]E. Munro, J. Orloff, R. Rutherford, and J. Wallmark, J. Vac. Sci. Technol. B **6**, 1971 (1988).